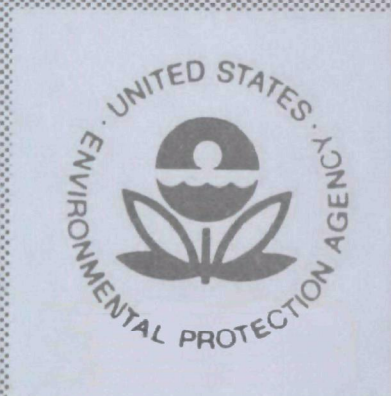


EPA-650/2-75-041

May 1975

Environmental Protection Technology Series

INFRARED SENSOR FOR THE REMOTE MONITORING OF SO₂



U.S. Environmental Protection Agency
Office of Research and Development
Washington, DC 20460

INFRARED SENSOR FOR THE REMOTE MONITORING OF SO₂

by

E. R. Bartle

SAI, Inc.
P. O. Box 1393
La Jolla, California 92037

Contract No. 68-02-1208
ROAP No. 26AAP
Program Element No. 1AA010

EPA Project Officer: Dr. H. M. Barnes

Chemistry and Physics Laboratory
National Environmental Research Center
Research Triangle Park, North Carolina 27711

Prepared for

U. S. ENVIRONMENTAL PROTECTION AGENCY
OFFICE OF RESEARCH AND DEVELOPMENT
WASHINGTON, D. C. 20460

May 1975

EPA REVIEW NOTICE

This report has been reviewed by the National Environmental Research Center - Research Triangle Park, Office of Research and Development, EPA, and approved for publication. Approval does not signify that the contents necessarily reflect the views and policies of the Environmental Protection Agency, nor does mention of trade names or commercial products constitute endorsement or recommendation for use.

RESEARCH REPORTING SERIES

Research reports of the Office of Research and Development, U.S. Environmental Protection Agency, have been grouped into series. These broad categories were established to facilitate further development and application of environmental technology. Elimination of traditional grouping was consciously planned to foster technology transfer and maximum interface in related fields. These series are:

1. ENVIRONMENTAL HEALTH EFFECTS RESEARCH
2. ENVIRONMENTAL PROTECTION TECHNOLOGY
3. ECOLOGICAL RESEARCH
4. ENVIRONMENTAL MONITORING
5. SOCIOECONOMIC ENVIRONMENTAL STUDIES
6. SCIENTIFIC AND TECHNICAL ASSESSMENT REPORTS
9. MISCELLANEOUS

This report has been assigned to the ENVIRONMENTAL PROTECTION TECHNOLOGY series. This series describes research performed to develop and demonstrate instrumentation, equipment and methodology to repair or prevent environmental degradation from point and non-point sources of pollution. This work provides the new or improved technology required for the control and treatment of pollution sources to meet environmental quality standards.

This document is available to the public for sale through the National Technical Information Service, Springfield, Virginia 22161.

Publication No. EPA-650/2-75-041

ABSTRACT

A prototype passive infrared sensor for the measurement of sulfur dioxide emissions from stationary sources is described. The infrared radiation emitted by gases in a plume originating from smokestacks may be detected, and from this the SO₂ concentration in the plume may be determined. In general, the radiation received by the sensor is a function of the intervening and background atmosphere. Thus, the problem of quantitative measurements is generally complex. A technique is described, based upon the principle of Gas Filter Correlation, which minimizes these effects.

This report presents a detailed description of the sensor, its specifications, and performance characteristics. The basic unit is battery operated and weighs only 10 kgms; thus, it is readily portable. Its sensitivity is presently limited to about 70 ppm-m for source plume temperatures of 270 C and about 290 ppm-m for temperatures of 170 C, but this can be improved.

The results of field testing at both oil and coal-burning power plants are compared with extractive sample data. In general, the remote measurements agree with the extractive data within ± 25 percent over SO₂ concentrations ranging from 150 ppm to 1300 ppm from slant ranges of 130 to 400 m.

This report is submitted in partial fulfillment of contract number 68-02-1208 by JRB Associates, a division of Science Applications, Inc. under the sponsorship of the Environmental Protection Agency.

CONTENTS

	PAGE
ABSTRACT	iii
TABLE OF CONTENTS	iv
ILLUSTRATIONS	v
TABLES	vi
ACKNOWLEDGEMENT	vii

SECTION

1	INTRODUCTION AND SUMMARY	1
	Statement of the Problem	1
	Brief Description of the Sensor	1
	Definitions, Symbols, and Units.	2
2	DESCRIPTION OF THE RGFC TECHNIQUE FOR REMOTELY DETECTING SO ₂	4
	Phenomenology	4
	Signal Calculations	6
	Theory of the GFC Technique.	9
3	SENSOR DESIGN AND PERFORMANCE	14
	Mechanical-Optical Design	14
	Electronics Design	16
	Theoretical Performance	18
	Laboratory Test Results and Calibration	21
	Field Testing	29
	Discussion of Field Test Data Reduction	32
	Conclusions	34
4	REFERENCES.	36
APPENDIX - Optimization of Gas Cell Parameters		37
	Theoretical	37
	Experimental	42

ILLUSTRATIONS

		PAGE
FIGURE		
1	Schematic of viewing geometry	5
2	Theoretically computed radiances of hot N ₂ -diluted SO ₂	8
3	Schematic diagram of remote gas filter correlation sensor	10
4	Optical system schematic	15
5	Signal processing block diagram	17
6	Radiance difference detected by sensor (assumes chopper's radiance is a 300 K blackbody)	20
7	Radiometric mode calibration for V _{2R} channel	22
8	Radiometric data compared with theoretical values	24
9	Data obtained with sensor operating in GFC mode (T = 270 C)	25
10	Data obtained with sensor operating in GFC mode (T = 170 C)	26
11	Data showing sensitivity of ratio to SO ₂ temperature and concentration	27
12	RGFC ratio mode calibration	28
13	Limiting sensitivity of the sensor for t = 90 seconds	30
14	Photograph of SO ₂ remote sensor during initial field testing	31
15	Comparison of remote sensing data with extractive data obtained from the DuPont analyzer and from EPA Method 6	33
A-1	Effect of specifying and reference cell optical thickness on sensor sensitivity	41
A-2	Theoretical calculation and measurement of N ₂ -diluted SO ₂ pressurized to one atm for SO ₂ sensor	44

TABLES

TABLE		PAGE
1	Summary of instrument parameters	19
2	Summary of remote SO ₂ field measurements made at two oil-burning power plants	29
3	Summary of remote SO ₂ field measurements made at a coal-burning power plant	32

ACKNOWLEDGEMENT

This report documents research and development performed by JRB Associates, a wholly-owned subsidiary of Science Applications, Incorporated, under Contract 68-02-1208 between 25 June 1973 and 28 February 1975. The work was sponsored by the Environmental Protection Agency, Research Triangle Park, North Carolina. The technical monitor was Dr. H. M. Barnes, Jr.

During this program valuable contributions were made by G. Houghton (mechanical-optical design), L. Acton (optical analysis), E. Meckstroth (electronics design, instrument assembly, testing, calibrations, and field measurements), G. Hall (electronics consultation), Dr. W. Malkmus (theoretical programming), and, especially, Dr. C. B. Ludwig (theoretical calculations, field testing, data analysis, and reporting).

SECTION 1

INTRODUCTION AND SUMMARY

STATEMENT OF THE PROBLEM

The goal of the program was to design, fabricate, calibrate, field test, and reduce the data for an infrared sensor that remotely measures sulfur dioxide emissions from stationary sources. The design goals were for the instrument to achieve the following performances:

Remote Range: 100-1000 meters (slant range)
Weight: less than 35 pounds
Volume: less than one cubic foot
SO₂ Concentration Range: 100-1000 ppm
Accuracy: $\pm 5\%$ for stack diameters of 1-10 meters.

The phenomenology for remote detection of pollutants emitted from stacks is dependent upon specific spectral measurements of infrared radiation. The infrared radiation emitted by gases in a plume originating from smokestacks may be detected, and from this the SO₂ concentration in the plume may be determined. In general, the radiation received by the sensor is a function of the intervening and background atmosphere. Thus, the problem of quantitative measurements is generally complex. A technique has been developed, based upon the principle of Gas Filter Correlation, which minimizes these effects.

BRIEF DESCRIPTION OF THE SENSOR

The infrared sensor for the remote monitoring of SO₂ is based upon the technique of Gas Filter Correlation described in Section 2 and elsewhere⁽¹⁻³⁾ in detail. Briefly, it is a modification of the Non-Dispersive Infra-Red (NDIR) technique that has been known for some time. It is based on the concept that a sample of gas provides a selective filter for radiation absorbed by a polluted mixture of atmospheric species. The radiation at the sensor is chopped so that it alternately passes through two optical paths, one through a cell containing the specific gas and one transparent. Thus, the radiation is modulated only at the wavelengths at which the pollutant absorbs and high specificity results.

It has been shown⁽¹⁾ that the signal generated by chopping between two cells is a non-linear function depending upon the SO₂ in the plume and fixed instrument parameters and the difference between the radiance emitted by the plume and background atmosphere. By ratioing two GFC signals

obtained using different amounts of SO₂ in the specifying cells, the effects of plume and atmospheric radiance are greatly minimized. As is shown, it is desirable to operate the sensor as a pure radiometer also. This is accomplished by blanking off the radiance from passing through the specifying gas cells.

Extensive laboratory testing was conducted and the gas cell parameters optimized. The sensitivity limits of the sensor were determined. Field tests were conducted at two oil-burning power plants and one coal-burning power plant under a variety of weather conditions. Extractive samples were taken and analyzed using EPA Method 6; these results were compared with the remote data and the two sets of data agreed within 25 percent.

DEFINITIONS, SYMBOLS, AND UNITS

a	ratio of spectral line half-width to line spacing
a_o	"a" divided by the equivalent pressure of the gas (atm ⁻¹)
f	aperture adjustment parameter, see Equations (15) and (16)
Δf	noise bandwidth of the sensor (Hz)
f(u), F(u)	defined by Equations (A-8) and (A-12)
k	monochromatic absorption coefficient (atm ⁻¹ -cm ⁻¹)
\bar{k}	mean absorption coefficient over a prescribed spectral interval $\Delta\lambda$ (atm ⁻¹ -cm ⁻¹)
ι	integration limits, see Equation (1) [length]
p	pressure (atm)
t	integration time (seconds)
u	optical thickness (atm-cm or ppm-m)
x	integration length
A, B	defined by Equation (A-6)
A_d	detector area (cm ²)
A_o	sensor entrance aperture (cm ²)
C	gas volumetric concentration
C(ω)	normalized spectral definition function of the sensor
D*	detector detectivity (cm-Hz ^{1/2} /W)

E	spectral energy arriving at sensor ($\text{W}/\text{cm}^2\text{-}\mu\text{m}\text{-sr}$)
L	optical pathlength (cm or m)
N^0	blackbody radiance ($\text{W}/\text{cm}^2\text{-}\mu\text{m}\text{-sr}$)
R	instrument responsivity ($\text{V}/\text{W cm}^{-2}\text{-sr}^{-1}$)
T	temperature ($^{\circ}\text{C}$ or $^{\circ}\text{K}$)
V	voltage generated at the detector by the energy passing through either the reference or specifying gas cell (V)
ΔV	ac voltage generated by alternately passing the energy through the two cells (V)
W, X, Y, Z,	defined by Equation (A-17)
ϵ	emissivity of a particular radiator
η	sensor overall efficiency
λ	wavelength (μm)
$\Delta\lambda$	spectral interval (μm)
τ	monochromatic transmittance of a particular instrument component or gaseous species
ω	wavenumber (cm^{-1})
ν	vibration transition parameter
Ω_0	solid angle entrance to the sensor (sr)

The sub and superscripts used are self-explanatory in the text.

A bar over a parameter indicates that it is the mean value over a spectral interval $\Delta\lambda$.

SECTION 2

DESCRIPTION OF THE REMOTE GAS FILTER CORRELATION TECHNIQUE FOR REMOTELY DETECTING SO₂

PHENOMENOLOGY

To illustrate the problem of remotely detecting SO₂ in stack plumes, consider a sensor receiving energy from a plume with the sky as the background (see Figure 1). From the basic theory of radiative transfer⁽⁴⁾, an expression is developed which describes the monochromatic radiation received by the sensor for the background, the effluent plume, and the intervening atmosphere:

$$\begin{aligned}
 E(\lambda) = & \tau_p \tau_a \int_{\infty}^{l_2} N_b^{O'}(T_b(x)) \frac{\partial \tau'_a(x)}{\partial x} dx \\
 & + \tau_a \int_{l_2}^{l_1} N_p^O(T_p(x)) \frac{\partial \tau_c(x)}{\partial x} dx \\
 & + \int_{l_1}^0 N_b^O(T_b(x)) \frac{\partial \tau_a}{\partial x} dx
 \end{aligned} \quad (1)$$

where the first term is the emission of the atmosphere from infinity to the far edge of the plume, the second term is the emission of the plume, and the third term is the emission of the atmosphere between the plume and the sensor.

$N^O(T(x))$ represents the blackbody function at temperature T , which is, in general, a function of x along the line of sight and, of course, is also a function of wavelength λ . The atmospheric transmission is indicated by the terms τ_a and τ'_a ; it consists of the transmissivities of all of the normal atmospheric species, i. e.,

$$\tau_a = \tau(\text{CO}_2) \times \tau(\text{H}_2\text{O}) \times \tau(\text{CH}_4) \times \tau(\text{N}_2\text{O}) \dots \quad (2)$$

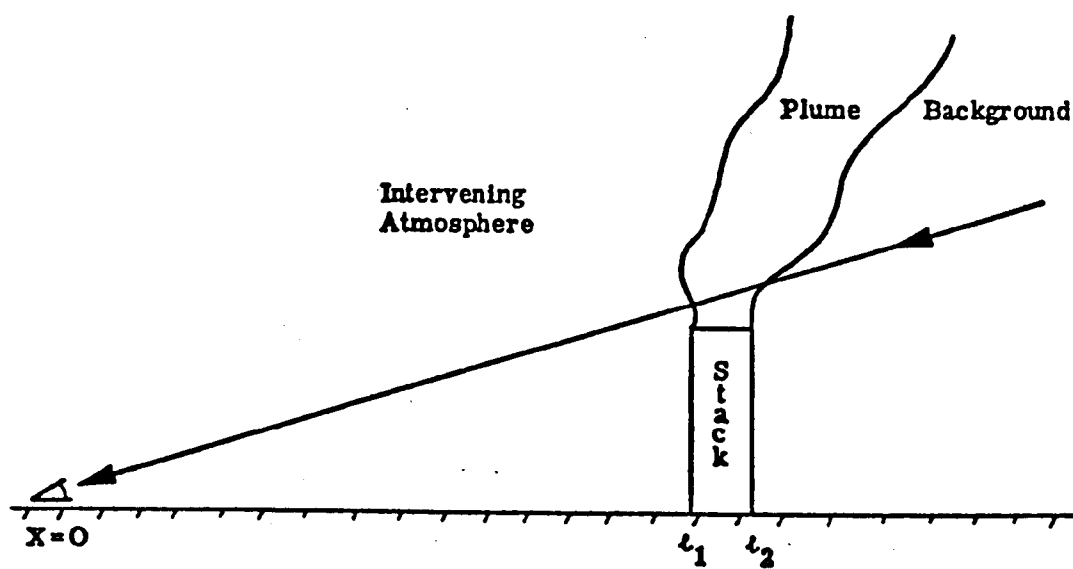


FIG. 1. Schematic of viewing geometry.

The transmissivity of the plume is similarly formulated

$$\tau_p = \tau(\text{SO}_2) \times \tau(\text{CO}_2) \times \tau(\text{H}_2\text{O}) \times \tau(\text{N}_2\text{O}) \times \tau(\text{CH}_4) \times \dots \quad (3)$$

This may be written as $\tau_p = \tau \tau_i$, where τ is the transmissivity due to SO_2 and τ_i is the transmissivity of all interfering species. The SO_2 transmissivity τ is given by

$$\tau = \exp - \int_{\lambda_2}^{\lambda_1} k(\lambda) C(x) p_t(x) dx \quad (4)$$

where $k(\lambda)$ is the spectral absorption coefficient of SO_2 , C is the unknown SO_2 concentration in the plume and p_t is the total pressure of the plume.

Consideration of Equations (1-4) shows that the task of quantifying the SO_2 concentration in the plume is complex. The radiation received by the sensor is a function of the atmospheric and plume temperatures as well as the emissivity of SO_2 and interfering species in the atmosphere and plume. In principle, it appears that a number of simple radiometric measurements over carefully chosen wavelength intervals and a suitable computer program may be used to obtain quantitative results. However, this is a very complex procedure and generally not sufficiently accurate. Therefore, we have devised a technique which is independent of the plume and atmospheric temperatures, and which does not require a computer to reduce the data.

SIGNAL CALCULATIONS

Sulfur dioxide possesses many infrared-active bands, two of which are the most promising ones. These are the $\nu_1 + \nu_3$ combination band centered at about $4 \mu\text{m}$ and the ν_1 fundamental band centered at about $8.6 \mu\text{m}$. Although the band at $8.6 \mu\text{m}$ is about 4 times stronger, it is heavily interfered by water vapor and—to a lesser extent—by CH_4 , N_2O and O_3 . On the other hand, only very weak interference occurs at $4 \mu\text{m}$ due to the presence of N_2O , CO_2 and CH_4 and the H_2O continuum. In addition, more sensitive IR detectors are available for operation at $4 \mu\text{m}$ than at $8.6 \mu\text{m}$. Thus, measurements at $4 \mu\text{m}$ are preferred.

In order to gain insight into the spectral emission levels of hot smokestack plumes containing SO_2 , we have calculated the radiance and emissivity of plumes, having various optical depths and temperatures. These calculations were performed with our line-by-line computer program, whose input parameters were taken from the AFCRL atlas of atmospheric lines and from data we have generated under different contracts⁽¹⁾.

From the listing of the SO₂ line parameters, it is determined that this band consists of many thousand lines. Besides SO₂ lines, there are those of N₂O and a few CO₂ and CH₄ lines. Water is present through the continuum, which is composed of the tails of strong lines originating in the 2.7 μm and 6.3 μm band systems.

In order to gain a better overview about the distribution and strength of the SO₂ band, we have generated the band model parameters, k and a_0 , averaged over 5 cm⁻¹ intervals. They are based on the statistical band model with exponential line strength distribution, viz.,

$$\tau(\text{SO}_2) = \exp \left[-ku/(1+ku/4a)^{-1/2} \right] \quad (5)$$

where u is the optical thickness ($= C_p L$) and $a = a_0 p_e$ where p_e is the equivalent pressure for N₂ broadened SO₂.

It is found that the SO₂ band at 4 μm is quite weak. Its band strength is only 22 cm⁻²atm⁻¹ at 300 K. In comparison, the ν₁ - SO₂ band at 8.7 μm is about 4 times stronger, the CO fundamental band at 4.6 μm is about 10 times stronger and the CO₂ band at 4.3 μm is over 100 times stronger. Thus, the emission of the hot smokestack gas is relatively weak at low SO₂ concentrations.

By multiplying the emissivities with the blackbody functions, the appropriate radiances are obtained. These calculations have been made for the particular narrow spectral bandpass filter used in the sensor. The calculated results are shown in Figure 2.

We have also used our computer program to calculate the typical transmission between a smokestack and an observer on the ground. For the conditions

Height of smokestack: 54 m
 Horizontal Distance: 122 m
 Relative Humidity: 85%
 Temperature: 16 C
 Concentration of N₂O: 0.3 ppm
 Concentration of CO₂: 320 ppm
 Concentration of CH₄: 1.4 ppm

the transmission becomes 0.9979, which indicates an insignificant loss due to atmospheric absorption. Even if the atmosphere were heavily polluted by SO₂, the transmission is decreased only slightly. As an example, 100 ppb of SO₂ reduces the transmission to only 0.9977.

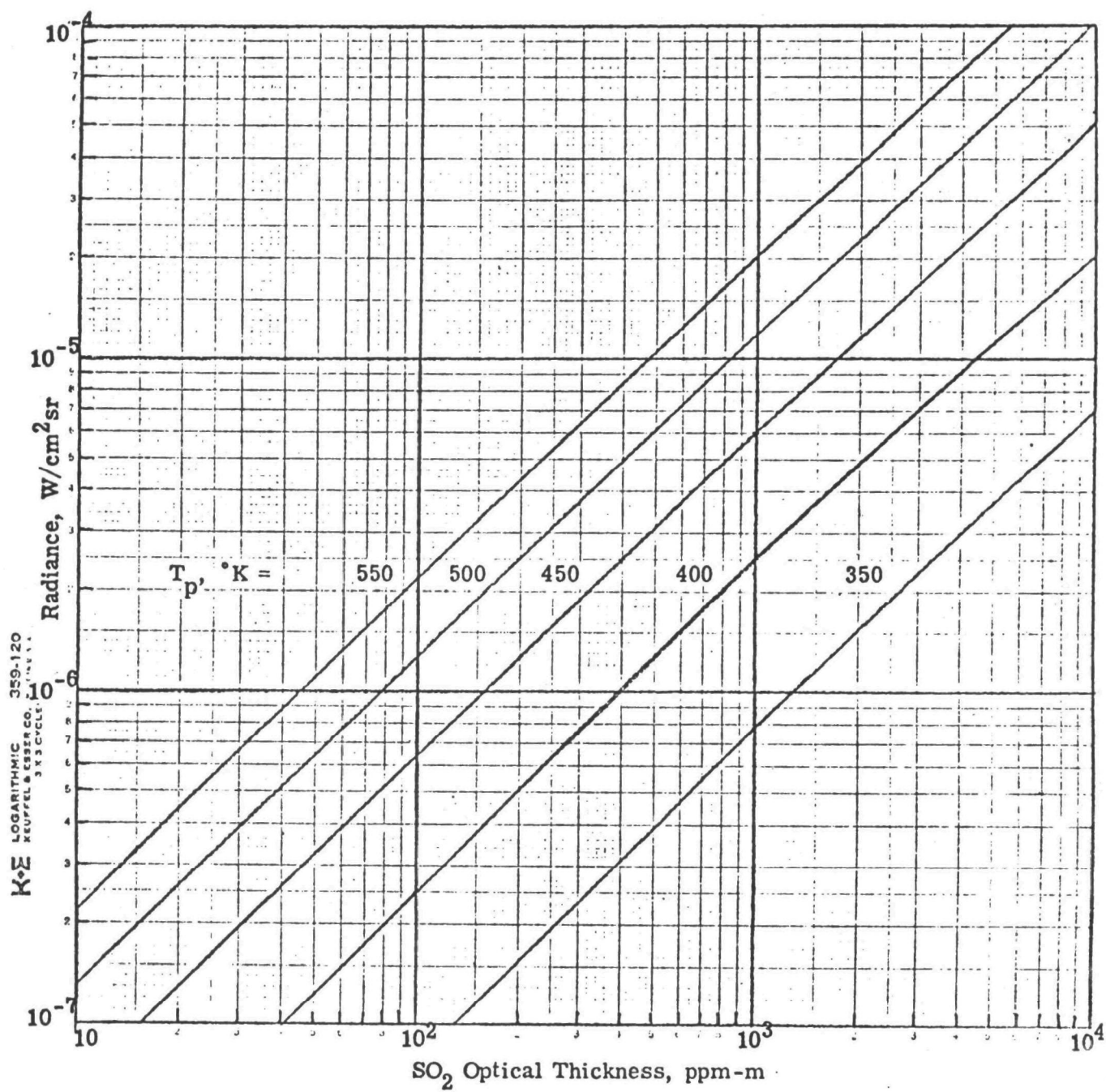


FIG. 2. Theoretically computed radiances of hot N_2 -diluted SO_2 .

THEORY OF THE GAS FILTER CORRELATION TECHNIQUE

Since 1969, we have been developing the Gas Filter Correlation (GFC) technique⁽¹⁻³⁾ which is a modification of the Non-Dispersive Infra-Red (NDIR) technique that has been known for some time⁽⁵⁾. In contrast to pure radiometry or dispersive spectroscopy, a GFC (non-dispersive) device uses the gas itself to obtain the ultimate high-spectral resolution filter (provided by the natural line-width of the gas). High spectral resolution is the most important parameter in obtaining specificity and accuracy in pollutant analysis.

Even quite narrow spectral bandpass radiometers are low-resolution instruments and specificity is difficult to obtain.

High-resolution instruments depend upon finding a single line of the pollutant to obtain specificity, but this necessitates the use of narrow apertures. Thus, sensitivity is difficult to obtain.

GFC combines the high energy throughput feature of radiometers and the high-resolution features of dispersive instruments. It makes use of the contributions of all spectral lines of a band system of a particular species to obtain sensitivity. Specificity is obtained by making use of random correlation between spectra arising from the particular species and interfering species; the principle of random correlation has been established⁽¹⁻³⁾ for most pollutant species and interfering species occurring naturally and in polluted atmosphere. In addition, a ratioing technique may be employed that eliminates effects of changes in source intensity, background radiation, and continuum absorption due to aerosols, water vapor, or other molecular species.

A remote GFC sensor consists basically of a single detector, a light chopper, a lens, a gas cell containing SO₂ and a reference cell (see Figure 3).

The chopper alternately passes the entering radiation through the gas cell and the reference cell. When the chopper is in the position indicated in Figure 3, the signal generated at the detector is

$$V_1 = \int_{\Delta\lambda} \{ E \tau_2 \tau_o \tau_3 + N_c^o \tau_2 \tau_r \tau_3 + \epsilon_1 N_1^o \tau_2 \tau_o \tau_3 + \text{ins} \} R d\lambda \quad (6)$$

where τ , N^o and ϵ refer to transmissivity, blackbody function and emissivity respectively; the numerical subscripts are indicated in Figure 3 and ins refers to the instrument which is maintained at a constant

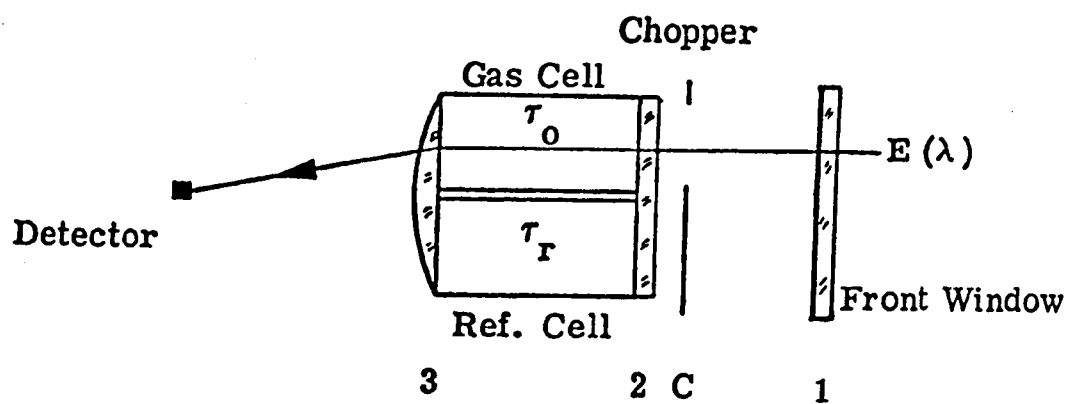


FIG. 3. Schematic diagram of remote gas filter correlation sensor.

temperature; R is the overall responsivity of the detector, optical efficiency and electronics. All symbols are, of course, a function of λ , but this is not noted for the sake of brevity.

Similarly, when the chopper blocks off the gas cell, the signal generated at the detector is

$$V_2 = \int_{\Delta\lambda} \left\{ E \tau_2 \tau_o \tau_3 + N_c^o \tau_2 \tau_r \tau_3 + \epsilon_1 N_1^o \tau_2 \tau_o \tau_3 + \text{ins} \right\} R d\lambda \quad (7)$$

The signal generated at the frequency of the forward chopper is the difference between V_2 and V_1 :

$$\Delta V = \int_{\Delta\lambda} \tau_2 \tau_3 [\tau_1 E + \epsilon_1 N_1^o - N_c^o] [\tau_r - \tau_o] R d\lambda \quad (8)$$

The instrument is balanced by replacing the incoming energy E by two calibration blackbody sources of temperatures T_{BB_1} and T_{BB_2} and τ_r is adjusted such that $\Delta V_{T_{BB_1}} = \Delta V_{T_{BB_2}}$. This implies $\bar{\tau}_r \approx \bar{\tau}_o$ where the bars denote mean values over the interval $\Delta\lambda$. But, since the values $\Delta V_{T_{BB_1}}$ and $\Delta V_{T_{BB_2}}$ are not electronically zero, in general, the value ΔV given in Equation (8) is always referenced against level $\Delta V_{T_{BB_1}}$ or $\Delta V_{T_{BB_2}}$. Since R , τ_2 , and τ_3 are only slowly varying functions of λ , an overall effective responsivity R_o may be defined by

$$R_o = \overline{\tau_2 \tau_3 R}$$

where the bar denotes the mean value over the interval $\Delta\lambda$. Thus,

$$\frac{\Delta V}{R_o} = \int_{\Delta\lambda} [\tau_1 E(\lambda) + \epsilon_1 N_1^o(\lambda) - N_c^o(\lambda)] [\tau_r - \tau_o(\lambda)] d\lambda \quad (9)$$

where $E(\lambda)$ is given by Equation (1). $\epsilon_1 N_1^o(\lambda)$ and $N_c^o(\lambda)$ are effectively eliminated through the balancing procedure; thus,

$$\frac{\Delta V}{R_o} = \int_{\Delta\lambda} E(\lambda) [\tau_r - \tau_o(\lambda)] d\lambda \quad (10)$$

When $E(\lambda)$ given by Equation (1) is introduced into Equation (10) and the integration over $\Delta\lambda$ carried out, one obtains, using the mean value theorem

$$\frac{\Delta V}{R_0} = \left. \begin{aligned} & \bar{\tau}_i \bar{N}_b^{O'} (\bar{\tau}_a - \bar{\tau}_a \tau'_a) (\bar{\tau} \tau_r - \bar{\tau} \tau_o) \\ & + \bar{N}_c^O [\bar{\tau}_a (\tau_r - \bar{\tau}_o) + \bar{\tau}_a \bar{\tau}_i (\bar{\tau} \tau_o - \bar{\tau} \tau_r)] \\ & + \bar{N}_b^O (1 - \bar{\tau}_a) (\tau_r - \bar{\tau}_o) \end{aligned} \right\} \quad (11)$$

Since by balancing the instrument, $\bar{\tau}_o = \tau_r$, Equation (11) may be simplified:

$$\frac{\Delta V}{R_0} = \bar{\tau}_i [\bar{\tau}_a \bar{N}_c^O - (\bar{\tau}_a - \bar{\tau}_a \tau'_a) \bar{N}_b^{O'}] (\bar{\tau} \tau_o - \bar{\tau} \tau_r) \quad (12)$$

Thus, an expression results that shows the ac signal is effectively a product of a modulation function that is only related to the SO_2 transmissivity and fixed instrument transmissivities and of the difference between the radiance emitted by the plume and background atmosphere.

If we now consider a second cell pair with $\bar{\tau}_o' \neq \bar{\tau}_o$ and chopped at a different frequency, but using the same detector and optical components, a similar expression is derived:

$$\frac{\Delta V'}{R_0} = \bar{\tau}_i [\bar{\tau}_a \bar{N}_p^O - (\bar{\tau}_a - \bar{\tau}_a \tau'_a) \bar{N}_b^{O'}] (\bar{\tau} \tau_o' - \bar{\tau} \tau_r') \quad (13)$$

Note, this modulation function has a different non-linear response from that given in Equation (12).

Division of Equation (12) by Equation (13) gives the signal to be observed,

$$S = \frac{\Delta V}{\Delta V'} = \frac{\bar{\tau} \tau_o - \bar{\tau} \tau_r}{\bar{\tau} \tau_o' - \bar{\tau} \tau_r'} \quad (14)$$

which is to a first order approximation independent of plume radiance, atmospheric radiance, intervening atmospheric transmissivity, and instrument spectral responsivity. Also, the ratioing of the responses from two GFC cell pairs gives a response function that is completely independent of

temperature if the gas cell and plume temperatures are the same. Any mis-match in these temperatures will cause only relatively small errors in determining SO₂ concentration due to the second order effects of temperature on the absorption coefficient of SO₂ and changes in spectral slope of the blackbody function with temperature.

The signal as a function of SO₂ concentration in the plume can be adjusted depending upon the amounts of SO₂ in the specifying cells. In addition, we have observed that the addition of a small amount of SO₂ to the reference cell will greatly enhance the sensitivity. In this case the signal is given by

$$S = \frac{\overline{\tau\tau_{02}} - \overline{\tau\tau_r} f_2}{\overline{\tau\tau_{01}} - \overline{\tau\tau_r} f_1} \quad (15)$$

where f_1 and f_2 are the dimensionless aperture attenuators used to balance or zero the sensor; viz.

$$\overline{\tau_{02}} = \overline{\tau_r} f_2 \quad \text{and} \quad \overline{\tau_{01}} = \overline{\tau_r} f_1 \quad (16)$$

The optimum values for $\overline{\tau_{01}}$, $\overline{\tau_{02}}$, and $\overline{\tau_r}$ were studied in detail. These results are presented in the Appendix.

SECTION 3

SENSOR DESIGN AND PERFORMANCE

MECHANICAL-OPTICAL DESIGN

The two-cell GFC pairs are contained in a single optical system as illustrated in Figure 4. Separate tuning fork choppers are used for each cell pair. The cells are 10 cm in length. The image of the stack plume is focused by an $f/3$ lens on a 1.0×1.0 mm detector which defines the field-of-view to be about 8 milliradians (8 m at 1 km). An ambient temperature operation (ATO) PbSe detector is used; but, a single-stage thermoelectric cooler is used to provide temperature control. A passband optical filter is located in front of the detector. This filter is centered at 4.00 microns with a half-transmission width of about 0.1 microns.

Sapphire optics, antireflection-coated, are used. A transmission of greater than 0.9 is obtained. The objective lens has a diameter of 5 cm and a focal length of 15 cm.

Section A-A of Figure 4 shows the configuration of the dual split cell. The two gas cells contain different partial pressures of SO_2 and are pressurized to 1 atm with pure N_2 to pressure-broaden the SO_2 lines. The reference cell contain a lesser amount of SO_2 pressurized to one atm with pure N_2 .

The tuning fork choppers, made by American Time Products (Bulova) are stable, reliable and low power. Because the frequency is dependent only on the mechanical resonance of the fork, no stable-frequency AC power source is needed and battery operation is possible, as is true of the entire electronics system.

Section B-B of Figure 4 shows the dual tuning fork configuration. Fork-1 is shown closed, allowing radiation to pass through the ΔV -1 reference cells; Fork-2 is shown open, allowing radiation to pass through the ΔV -2 gas cell. Fork-1 operates a frequency of 40 Hz and Fork-2 at a frequency of 100 Hz. Because a single lens serves both ΔV -1 and ΔV -2 systems and superimposes the image of each on the same detector, both systems have exactly the same field-of-view at the stack plume, as is essential for proper cancellation of the stack effluent temperature factor. The superimposed image signals of the two ΔV systems are electronically separated by signal processing described later.

A third tuning fork chopper, operating at 800 Hz, is located immediately ahead of the detector aperture. This chopper obstructs the entire beam when

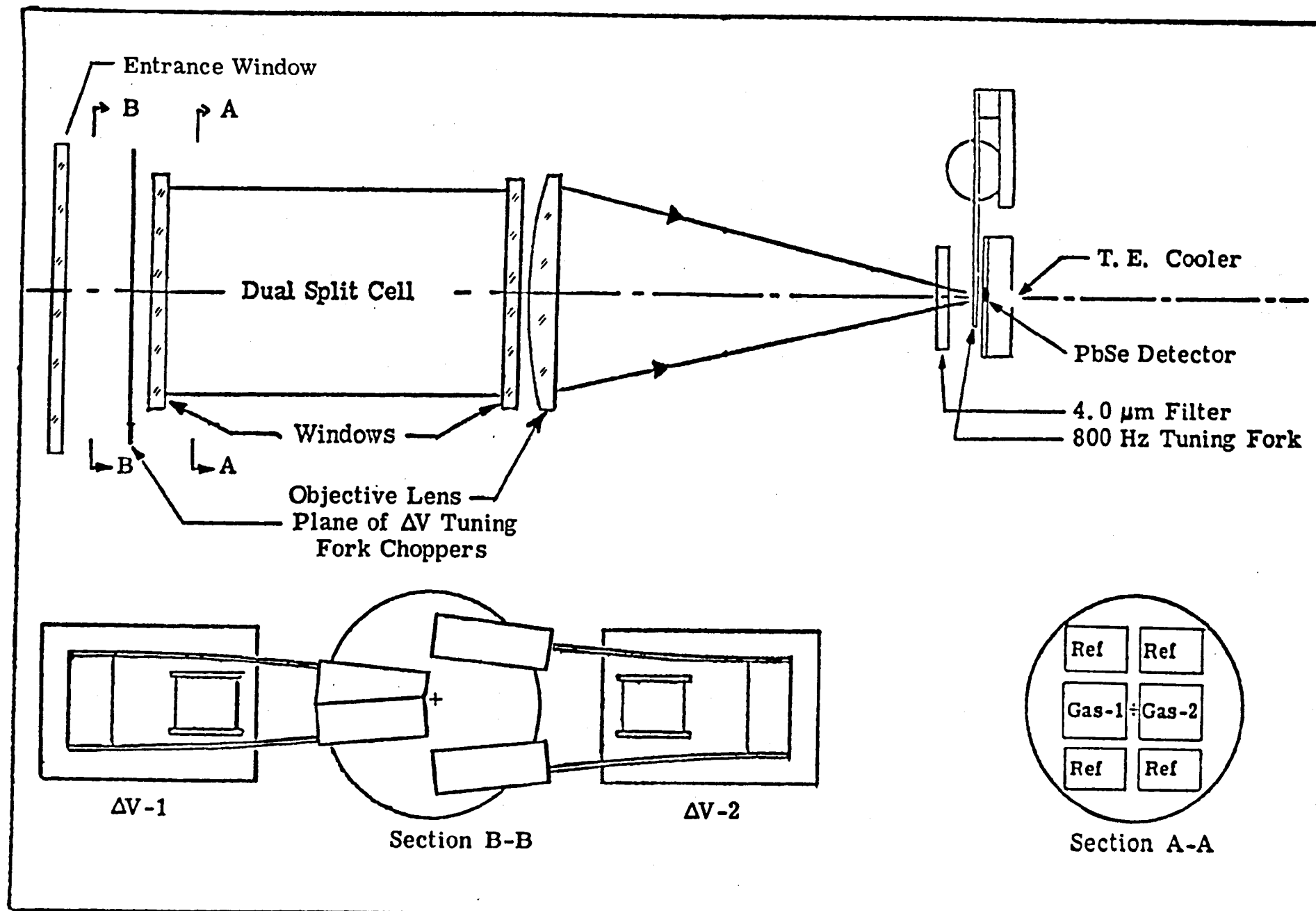


FIG. 4. Optical system schematic.

closed. The purpose of this chopper is to eliminate the low frequency $1/f$ detector noise from the ΔV signals.

Because of the small (8 mr) field-of-view, accurate aiming is essential. A 4-power Bushnell riflescope, accurately aligned with the GFC optics, is an integral part of the instrument. An illuminated retical in the riflescope permits accurate aiming at dusk or under other adverse lighting conditions.

ELECTRONICS DESIGN

An electronic signal processing technique that involves phasing, gating (sample-hold) and ratioing of different frequency signals has been developed. A block diagram of the electronics is shown in Figure 5.

In this instrument, two ΔV signals are used resulting from the use of two gas/reference cells systems containing different partial pressures of SO_2 . Each cell pair is chopped by a tuning fork chopper of different frequency. Because of the common objective lens the image at the detector consists of both ΔV signals at their respective chopping frequencies. These are later separated by electronic filtering. The frequencies are 40 Hz and 100 Hz. These are not harmonically related and are far enough apart to allow good separation by filtering, yet are low compared with the 800 Hz "carrier" system created by the third chopper, described below. This tuning fork chopper, operating at 800 Hz, is located immediately in front of the aperture plate and obstructs the entire light beam when closed. The detector signal is therefore the 800 Hz "carrier" signal amplitude modulated by the two ΔV chopper frequencies.

The detector is followed by a preamp and a 800 Hz bandpass filter. The filter passes the 800 Hz signal and its modulation side-bands at 700, 760, 840 and 900 Hz while rejecting the DC component of the detector output which is due to the bias current. Thus, even though low frequency ΔV chopping is needed in order to obtain large-amplitude fork oscillations, only the detector noise at the 800 Hz passband is processed, and the large $1/f$ detector noise at the low ΔV chopping frequencies is rejected and high effective detector D^* 's are obtained.

The filter output feeds a lock-in amplifier. Receiving its reference signal from the 800 Hz fork driving circuit, the lock-in synchronously detects the 800 Hz wavetrain and provides a DC output on which are superimposed the two ΔV signals.

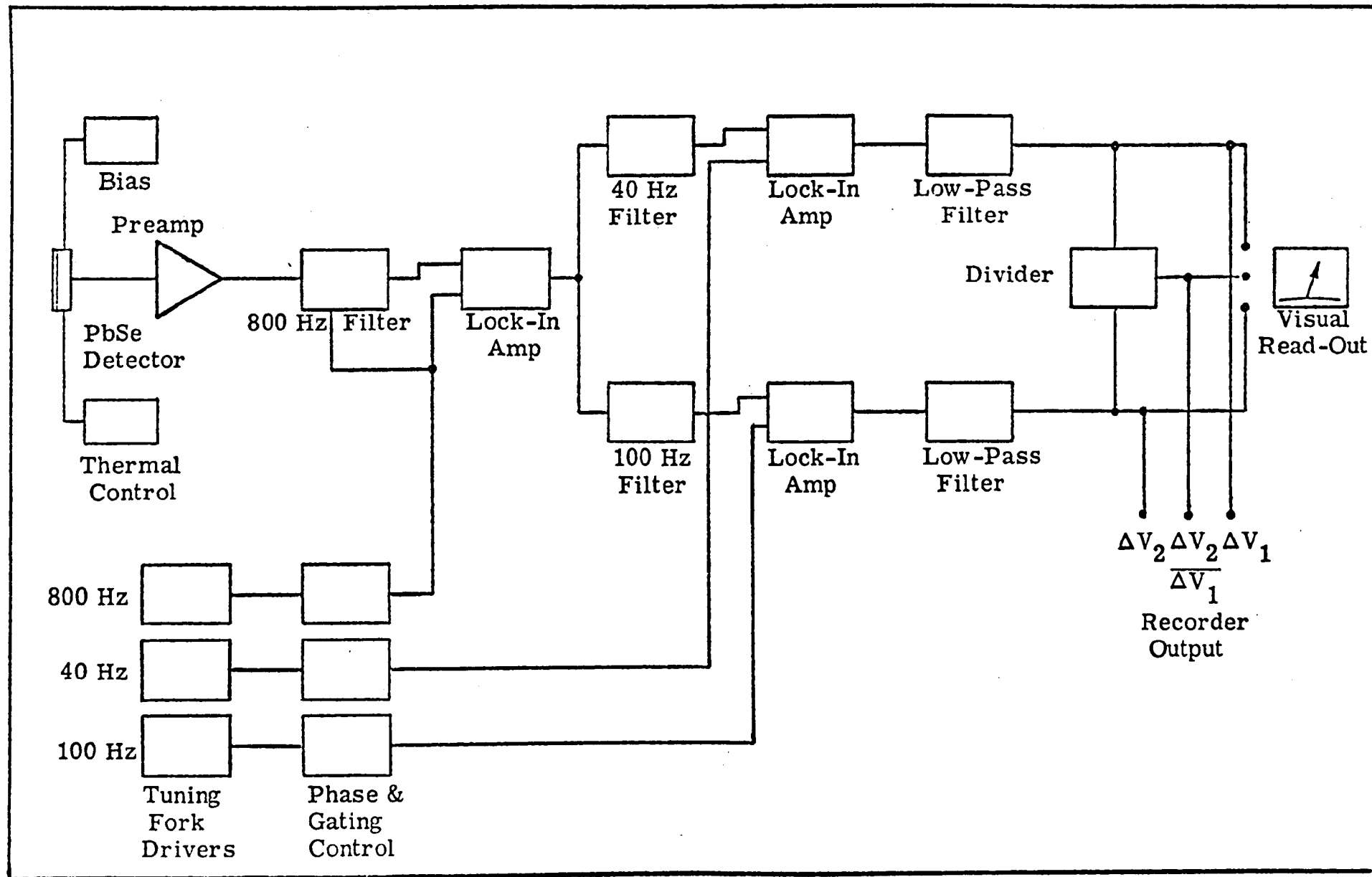


FIG. 5. Signal processing block diagram.

THEORETICAL PERFORMANCE

The signal-to-noise ratio for a GFC radiometer is given by

$$\text{SNR} = \frac{\eta \bar{\tau}_o A_o \Omega_o D^* \Delta E \Delta \lambda}{\sqrt{A_d \Delta f}} \quad (17)$$

where

- η is the instrument efficiency
- $\bar{\tau}_o$ is the transmissivity through the SO₂ gas cell
- A_o is the entrance aperture of the gas cell (cm²)
- Ω_o is the instrument acceptance solid angle (sr)
- D^* is the detector detectivity (cm-Hz^{1/2}/W)
- A_d is the detector area (cm²)
- Δf is the electronic bandpass (Hz)
- ΔE is the difference in radiance between the instrument gas and vacuum cells (W/cm²-μ-sr)
- $\Delta \lambda$ is the bandpass of the optical filter

A figure of merit for any radiometric instrument is the noise-equivalent-spectral-radiance which is given by Equation (17), setting SNR = 1; thus,

$$\text{NEN} = \frac{\sqrt{A_d \Delta f}}{\eta \bar{\tau}_o A_o \Omega_o D^*}, \text{ W/cm}^2\text{-sr} \quad (18)$$

A summary of the instrument parameters is given in Table 1.

Calculations of the radiance integrated over the actual filter band-pass were made. The results are presented in Figure 2. Operating as a pure radiometer (channel 2), the difference between these radiances and the radiance of the forward chopper is indicative of the signal to be detected. For example, if the chopper is emitting as a 300 K blackbody, the radiance difference is plotted in Figure 6. Since the theoretical NEN for Channels 1 and 2 are 1.22×10^{-7} and 8.14×10^{-8} W/cm²sr, respectively, the theoretical radiometric sensitivities are on the order of 150 ppm-m and 100 ppm-m for a temperature of 350 K.

TABLE 1
SUMMARY OF INSTRUMENT PARAMETERS

Parameter	Channel 1	Channel 2
η *	0.37	0.37
$\bar{\tau}_O$ **	0.44	0.66
f, Hz	100	40
A_O , cm ²	1.54	1.54
Ω_O , sr	6.4×10^{-5}	6.4×10^{-5}
D^* , cm Hz ^{1/2} /W	2.7×10^9	2.7×10^9
A_d , cm ²	10^{-2}	10^{-2}
Δf , Hz	2.8×10^{-3} to 0.25	2.8×10^{-3} to 0.25
NEN, W/cm ² -sr ***	1.221×10^{-7}	8.143×10^{-8}

* $\eta = \tau_{\text{window}} \times \tau_{\text{gas cell window}} \times \tau_{\text{lens}} \times \tau_{\text{filter}} \times \eta_{\text{electronics}}$
 $= .98 \times (.90)^2 \times .95 \times .5 \times .98 = 0.37$

** See Appendix.

*** Assumes integration time = 90 seconds; $\Delta f = 1/4 t = 2.8 \times 10^{-3}$ Hz.

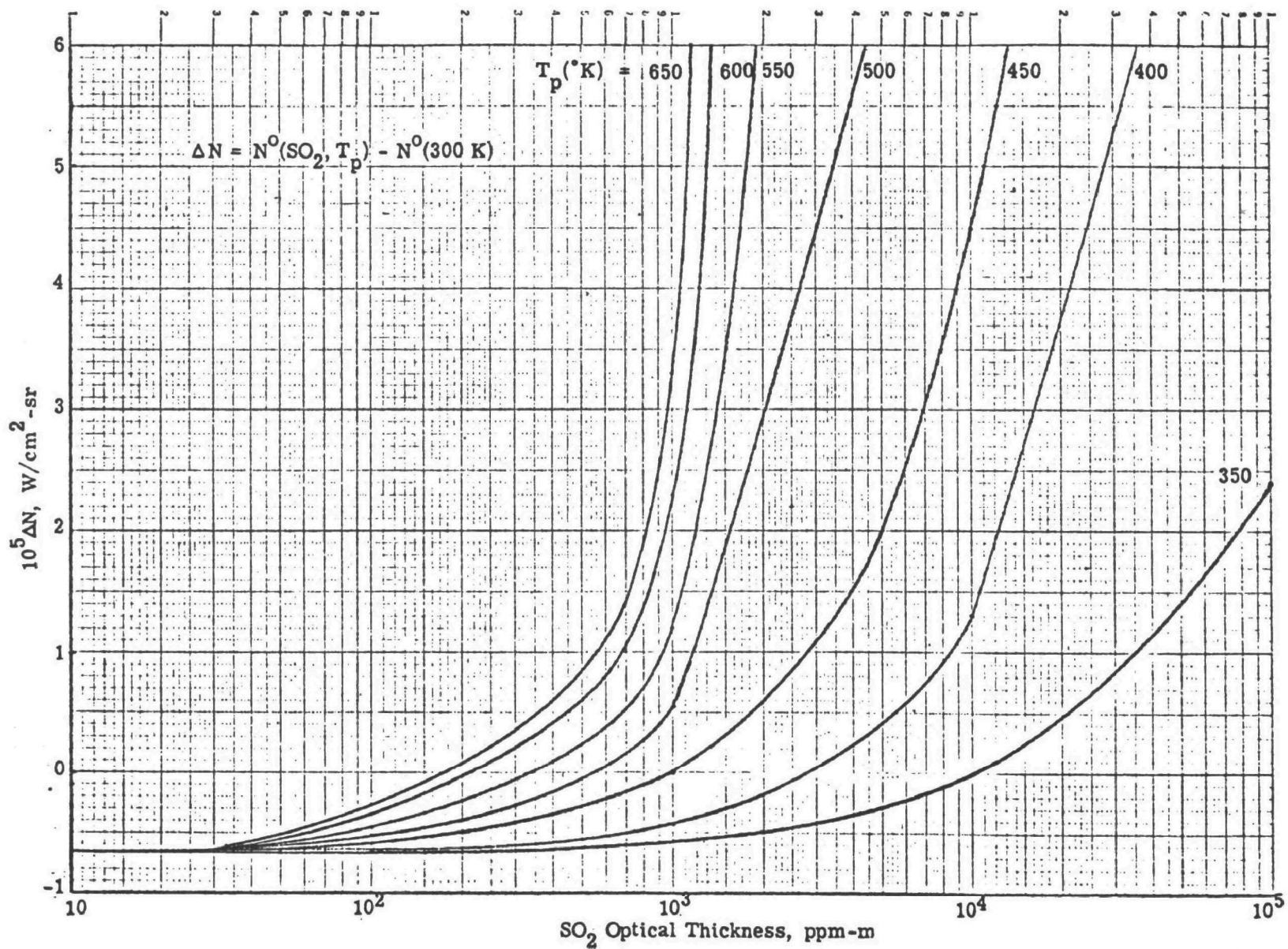


FIG. 6. Radiance difference detected by sensor (assumes chopper's radiance is a 300 K blackbody).

LABORATORY TEST RESULTS AND CALIBRATION

Testing of the sensor was performed to determine the optimum specifying and reference cell SO₂ concentration. The optimum concentrations and corresponding transmissivities are:

$$\begin{array}{ll} u_{01} = 5.0 \text{ atm-cm} & \bar{\tau}_{01} = 0.44 \\ u_{02} = 2.0 \text{ atm-cm} & \bar{\tau}_{02} = 0.66 \\ u_r = 0.5 \text{ atm-cm} & \bar{\tau}_r = 0.88 \end{array}$$

Measurements were made of the signal and noise of the sensor, while operating in the radiometric mode and in the GFC mode.

A Barnes Model 1140T Field Source was used to calibrate channel 2 (V_{2R}) operating as a pure radiometer. The results, covering a temperature range from 50 to 225 C, are presented in Figure 7. Note, these results are for the sensor normalized to— Gain = 10 and Attenuation = 10.

In order to compare the experimental data with theoretical predictions, we have to determine the instrument responsivity. The radiometric responsivity R₀ is defined through

$$V_{2R} = R_{02} \int_{\Delta\omega} C(\omega) [N^0(\omega, T) - N^0(\omega, T_C)] d\omega \quad (19)$$

where V is the radiometer signal in volts, R₀ is the responsivity in V/W cm⁻²sr⁻¹, C(ω) is the normalized filter function, and N⁰(ω, T) and N⁰(ω, T_C) are the blackbody functions of the calibration source and chopper blade, respectively.

From the measurements of V_{2R}, the radiometric responsivity was determined—

$$R_{02} = 7.0 \times 10^3 \text{ V/W cm}^{-2}\text{sr}^{-1} \quad (20)$$

The measured peak-to-peak noise level with an integration time of 90 seconds is 5×10^{-3} V. This is equivalent to $5 \times 10^{-3}/5 (= 10^{-3} V_{\text{rms}})$, assuming a factor of 5 to convert peak-to-peak random noise to rms noise; i. e., 99 percent of the noise energy exists within a voltage range of $5 \times V_{\text{rms}}$. The theoretically predicted noise, given by the NEN in Table 1, is $8.14 \times 10^{-8} \times 7.0 \times 10^3 = 5.7 \times 10^{-4} V_{\text{rms}}$. Thus, the sensor's noise limit is about two times higher than predicted. The actual rms noise measurements converted into radiance is $7.1 \times 10^{-8} \text{ W/cm}^2\text{-sr}$. This defines the minimum detectable SO₂ optical thickness.

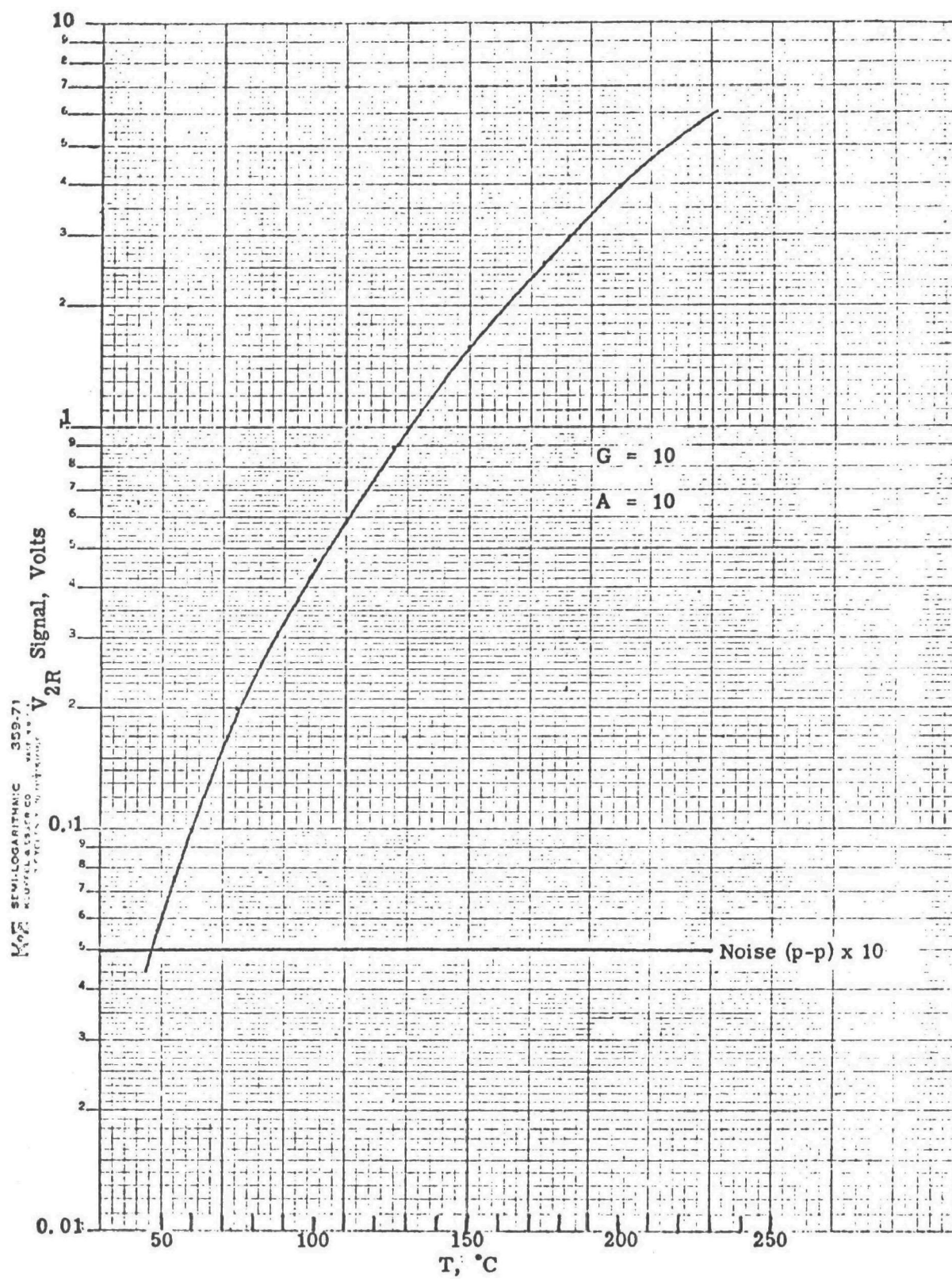


FIG. 7. Radiometric mode calibration for V_{2R} channel.

Measurements were also made of N₂-diluted SO₂ mixtures heated to 170 and 270 C in a 50 cm calibration cell with 7.5 cm dia. sapphire windows (transmissivity = 0.88). The experimental data corrected for window emission are plotted in Figure 8; also shown are the theoretically predicted values obtained by multiplying $R_0 (= 7 \times 10^3 \text{ V/W cm}^{-2}\text{-sr}^{-1})$ with the radiance differences given in Figure 6. Excellent agreement is obtained.

Thus, by using the curves presented in Figure 2, the radiance of the choppers, and the empirical value of R_0 (Equation (20)), the SO₂ optical thickness may be determined from field radiometric measurements, if the plume temperature is known, or vice-versa.

Operating in the GFC mode, the sensor is first balanced by adjusting the reference cell apertures such that the same ΔV signal levels are obtained when viewing the field source at temperatures of 350 and 500 K. Note, this is not necessarily electronic zero. After balancing, measurements were made of N₂-diluted SO₂ mixtures heated to 170 and 270 C in the 50 cm calibration cell.

Preliminary measurements were made with a small (0.25 x 0.25 mm) detector which provides a sensor fov of 2 mrad. The initial measurements were made with pure N₂ in the reference cells and with $u_{01} \approx 4.3 \text{ atm-cm}$ and $u_{02} \approx 1.3 \text{ atm-cm}$. Tests were conducted by using the laboratory atmosphere as the background and by placing a dry ice block behind the cell simulating a cold sky background; no discernible differences in the data were observed in the two test procedures.

Experimental data of ΔV_1 and ΔV_2 were obtained at temperatures of 270 C and 170 C and are reproduced in Figures 9 and 10. The abscissa is the optical thickness of SO₂ in ppm-m. In dividing ΔV_2 by ΔV_1 , the ratio which is independent of the gas temperature, is obtained. The results are shown in Figure 12. As expected, the results are independent of the temperature. These experiments demonstrate the viability of the ratio technique for the measurement of hot SO₂ emission without knowing the gas temperature. The resulting calibration data (Figure 11) were used to interpret field measurements at two oil-burning plants, as described in the following section.

Latter field measurements and laboratory experiments showed that the $\Delta V_2/\Delta V_1$ ratio could be made more sensitive by optimizing the gas-reference cells' SO₂ optical thicknesses. Using near optimum values, a calibration curve was obtained (see Figure 12) that was applicable to field measurements at a coal-burning power plant.

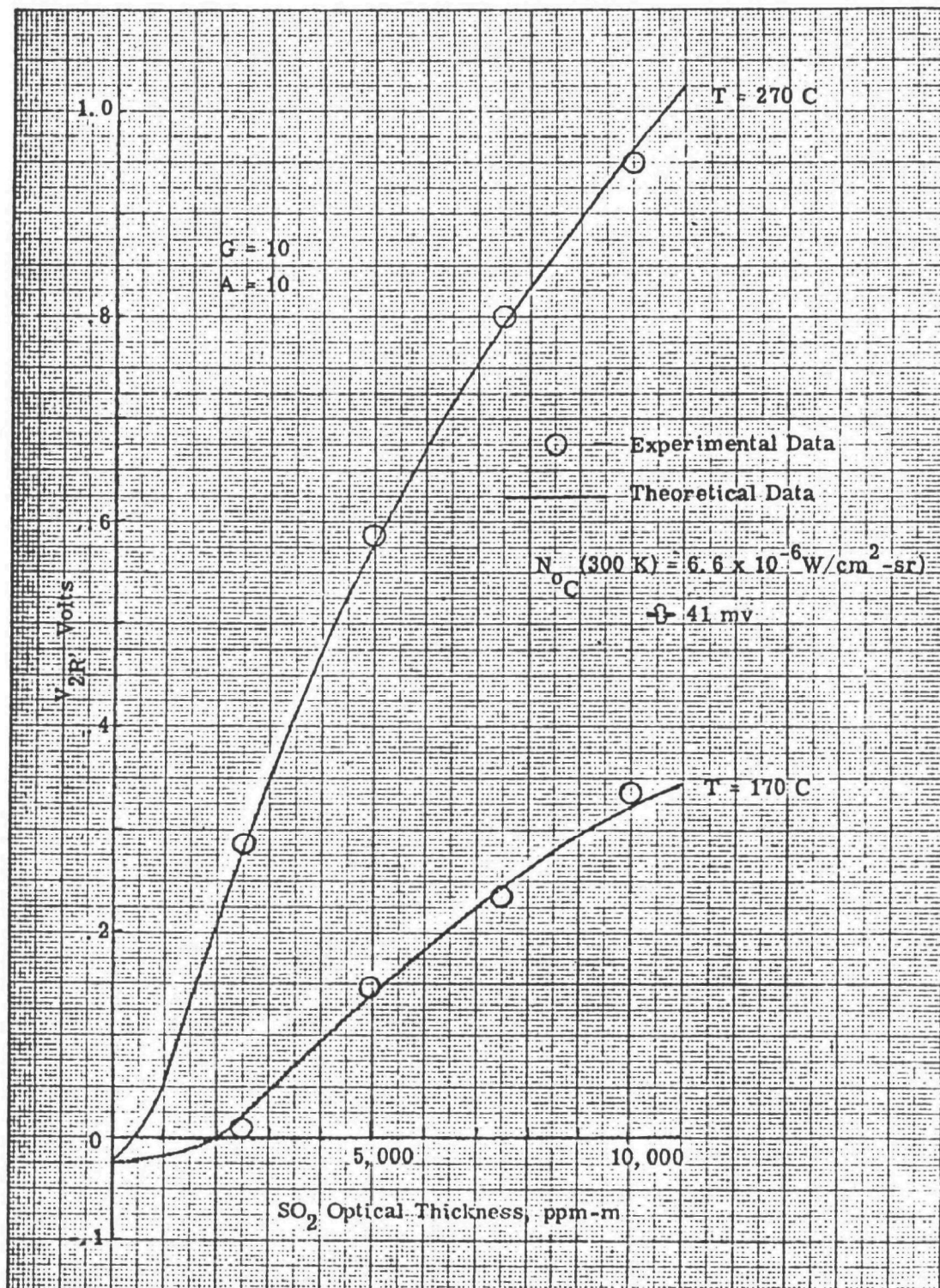


FIG. 8. Radiometric data compared with theoretical values.

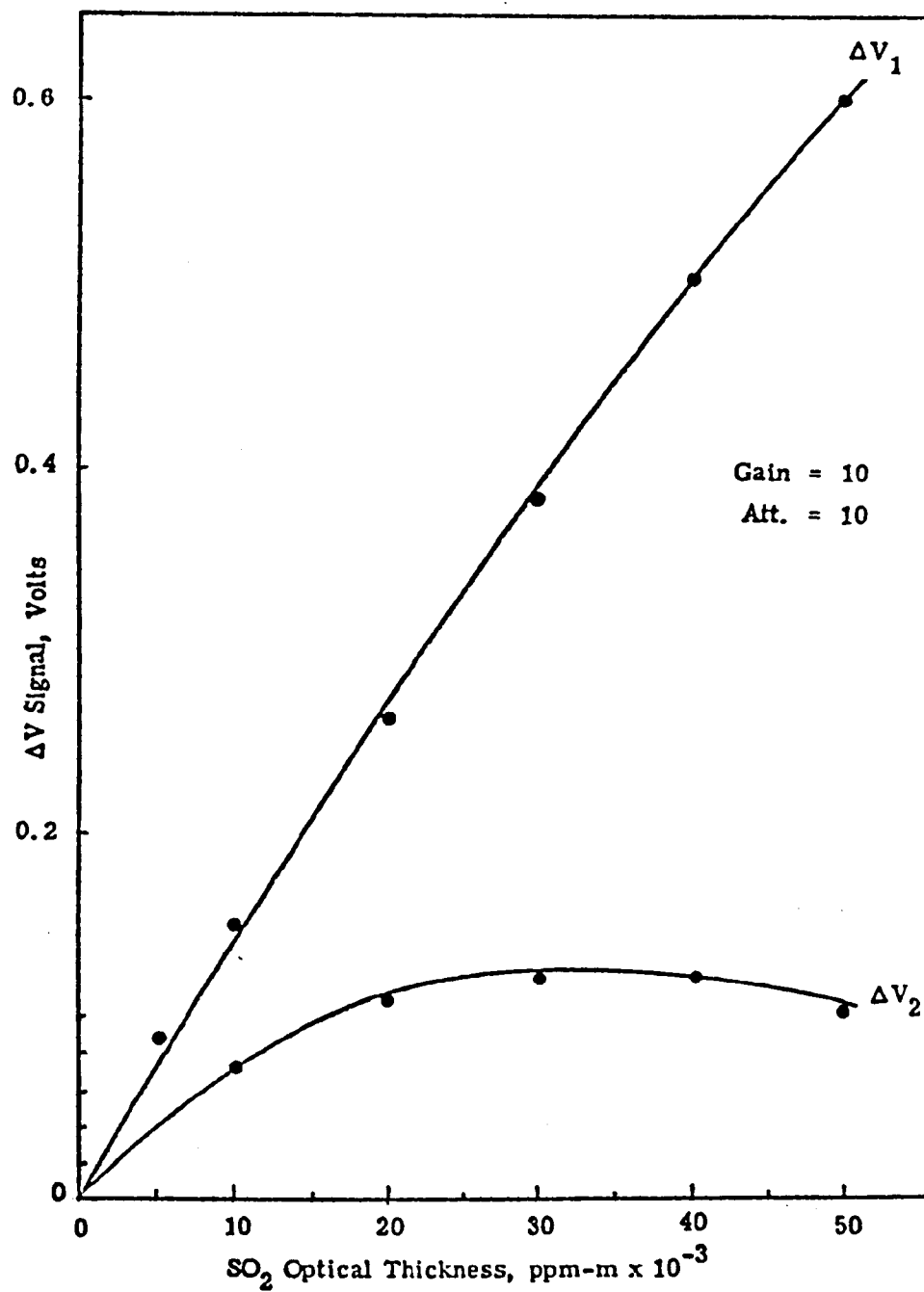


FIG. 9. Data obtained with sensor operating in GFC mode ($T = 270^\circ\text{C}$).

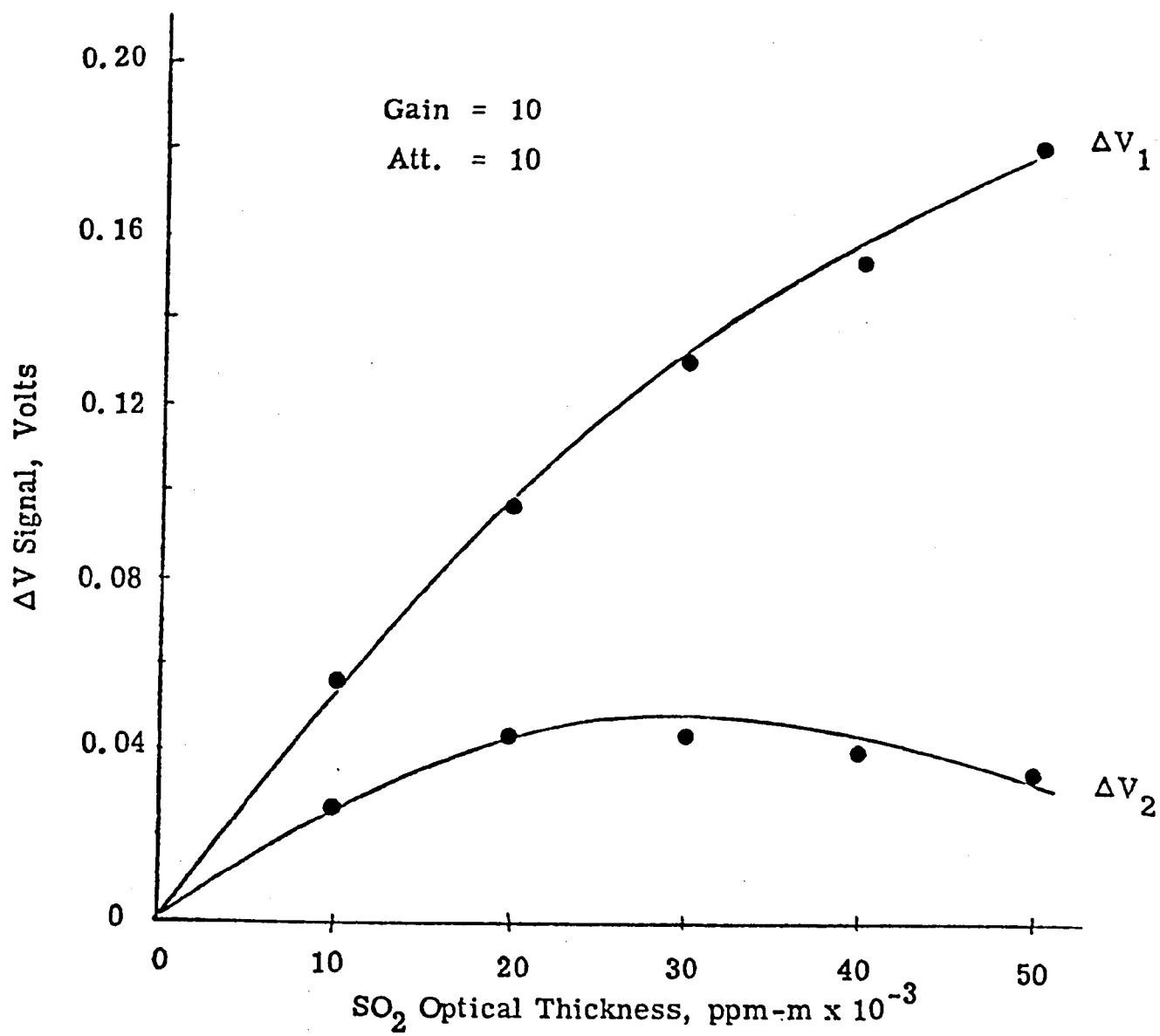


FIG. 10. Data obtained with sensor operating in GFC mode (T = 170 C).

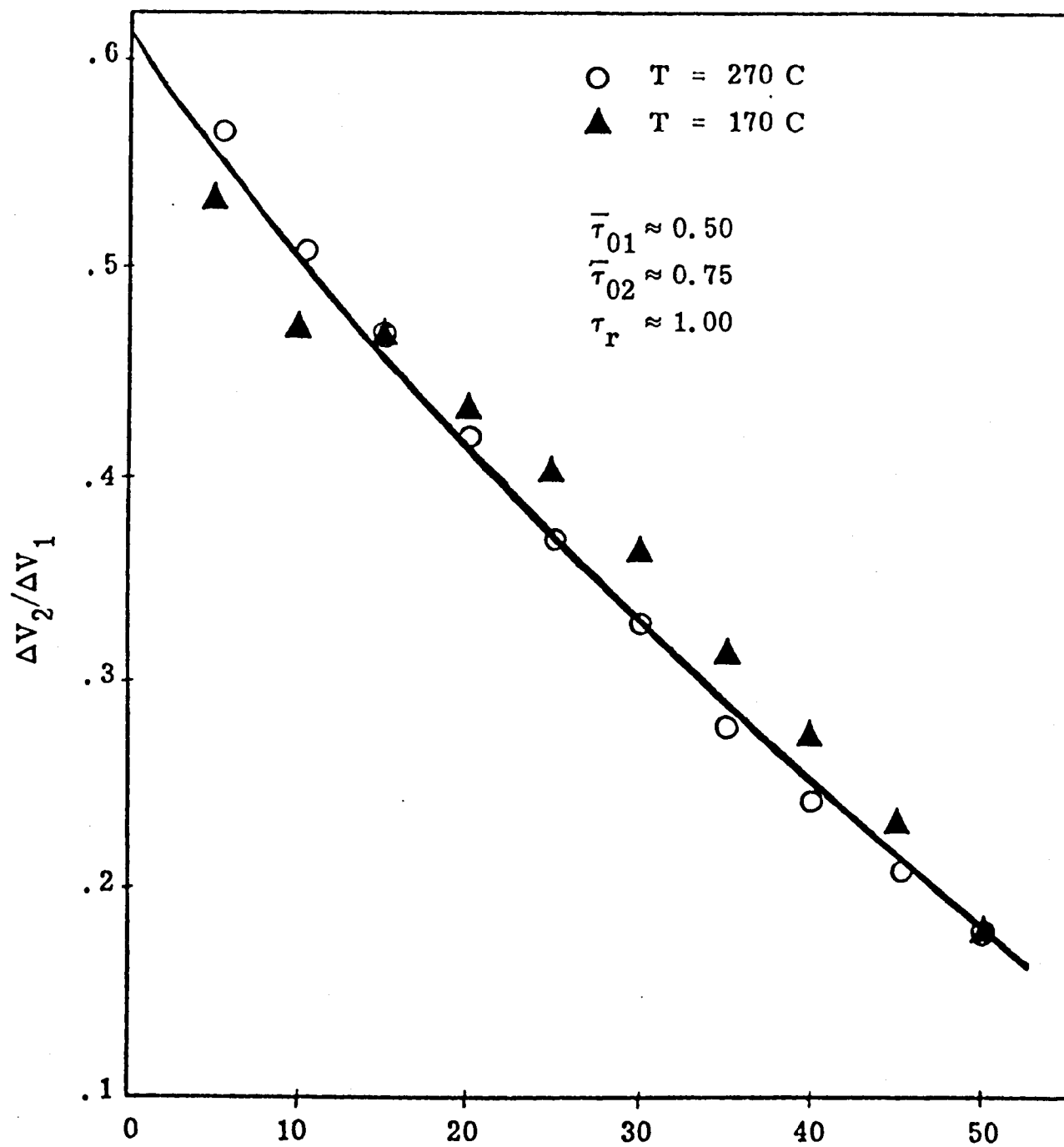


FIG. 11. Data showing sensitivity of ratio to SO_2 temperature and concentration.

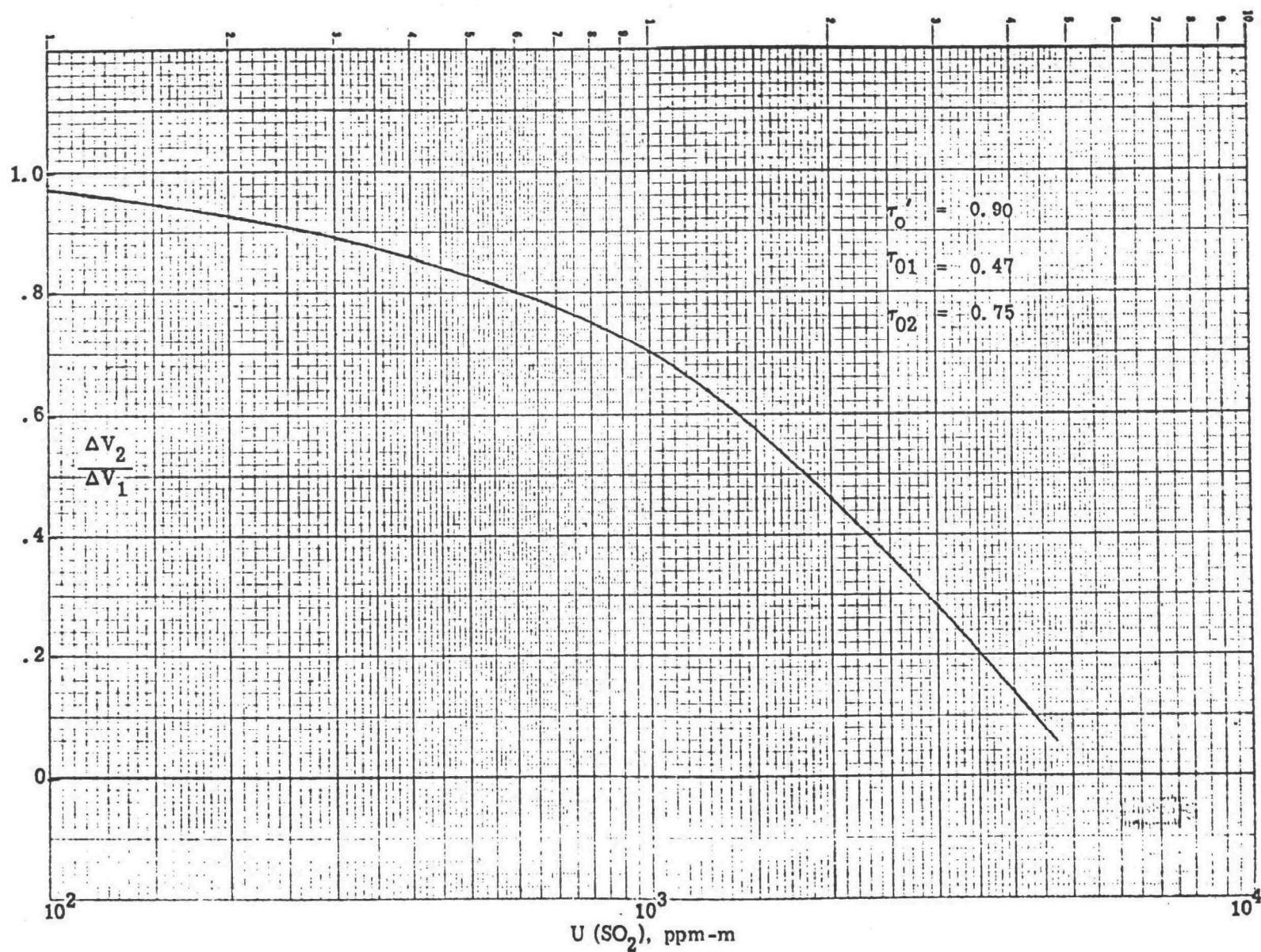


FIG. 12. RGFC ratio mode calibration.

From the measurements of signal and rms noise of the sensor, its limiting sensitivities as a function of plume temperature have been established. The results are given in Figure 13. These results are based on an integration time equal to 90 seconds and, for the radiometric mode, assume the chopper radiates as a blackbody at a temperature of 300 K; they are based upon the condition when the signal-to-rms noise ratio equals one.

FIELD TESTING

Preliminary field measurements were made using the 0.25 x 0.25 mm detector and non-optimized gas cell parameters at two oil-burning power plants near San Diego, CA. A photograph of the first site is shown in Figure 14. A summary of these measurements is presented in Table 2. Extractive measurements analyzed using EPA Method 6 were made during all tests except the first one.

TABLE 2
SUMMARY OF REMOTE SO₂ FIELD MEASUREMENTS
MADE AT TWO OIL-BURNING POWER PLANTS

Date	Range	Stack Dia.	Fuel	Temp.	SO ₂ Conc. Range	Weather Conditions, Time
3/25/74	130 m	4.25 m	oil	650 K	~ 200 ppm	20 C, calm, partial clouds, p. m.
5/20/74	185 m	4.0 m	oil	410 K	350-450 ppm	21 C, light wind, clear, p. m.
5/21/74	185 m	4.0 m	oil	420 K	260-340 ppm	26 C, light wind, partial clouds, p. m.
5/21/74	130 m	4.0 m	oil	420 K	170-230 ppm	26 C, light wind, partial clouds, p. m.
5/23/74	130 m	4.0 m	oil	440 K	260-340 ppm	22 C, calm, clear, dusk

The data taken on 3/23/74 are consistent with a nearly steady SO₂ concentration in the stack of about 200 ppm, which was a calculated value based upon the known sulfur content of the fuel oil⁽⁷⁾. (No extractive data were available during these first tests.) However, the accuracy at these low SO₂ concentrations is low (see calibration curve in Figure 11). Radiometric mode data were also taken and reduced, using laboratory calibration curves and the measured in-stack temperature; the results indicate a concentration range from 150 to 210 ppm SO₂.

The data taken on 5/20, 5/21 and 5/23 were obtained at the second site. In these cases the plume temperatures were lower, as seen by the data in Table 2, and the signal levels were correspondingly low, giving the larger indicated uncertainties in the data. Extractive data were taken

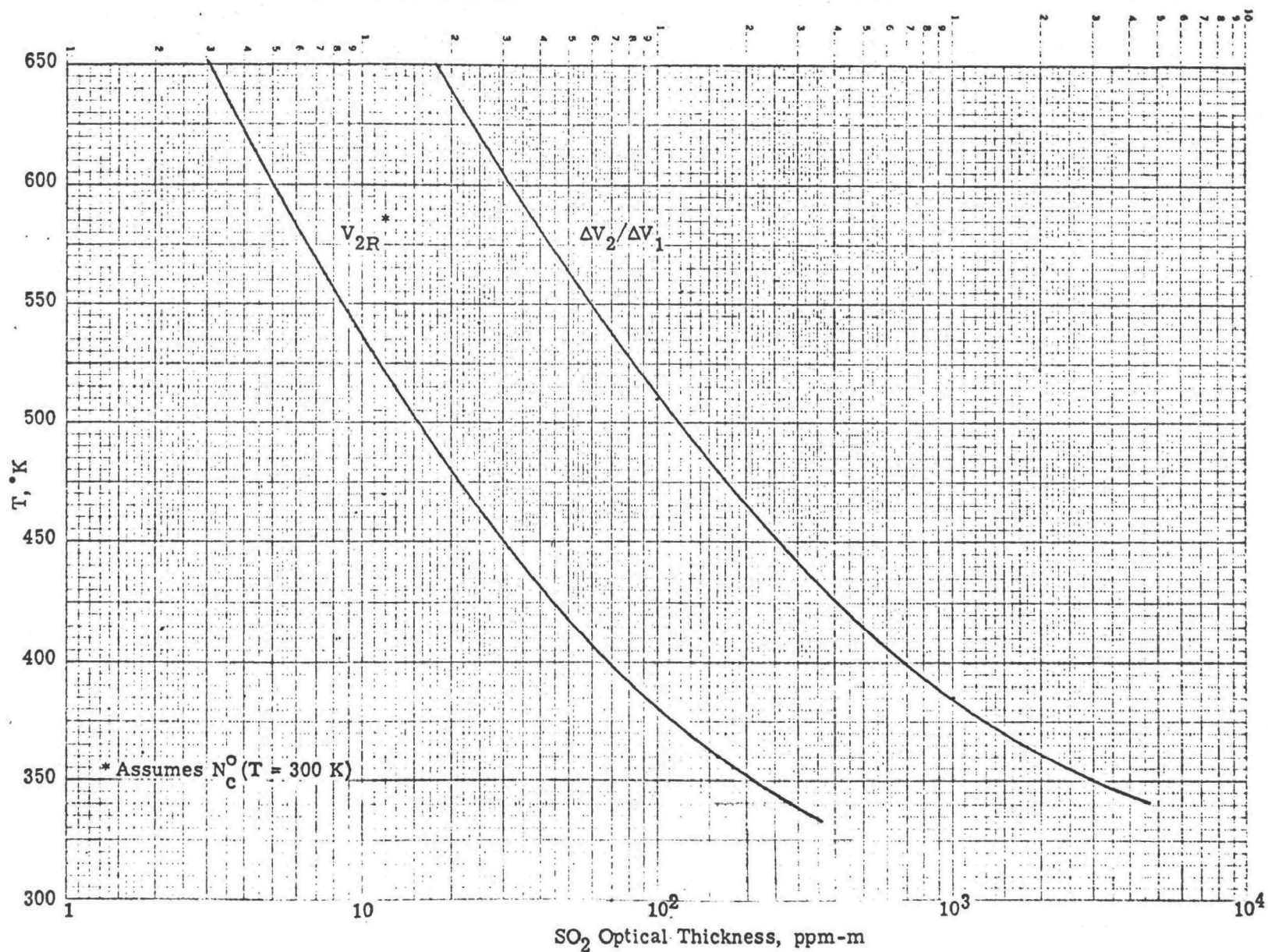


FIG. 13. Limiting sensitivity of the sensor for $t = 90$ seconds.

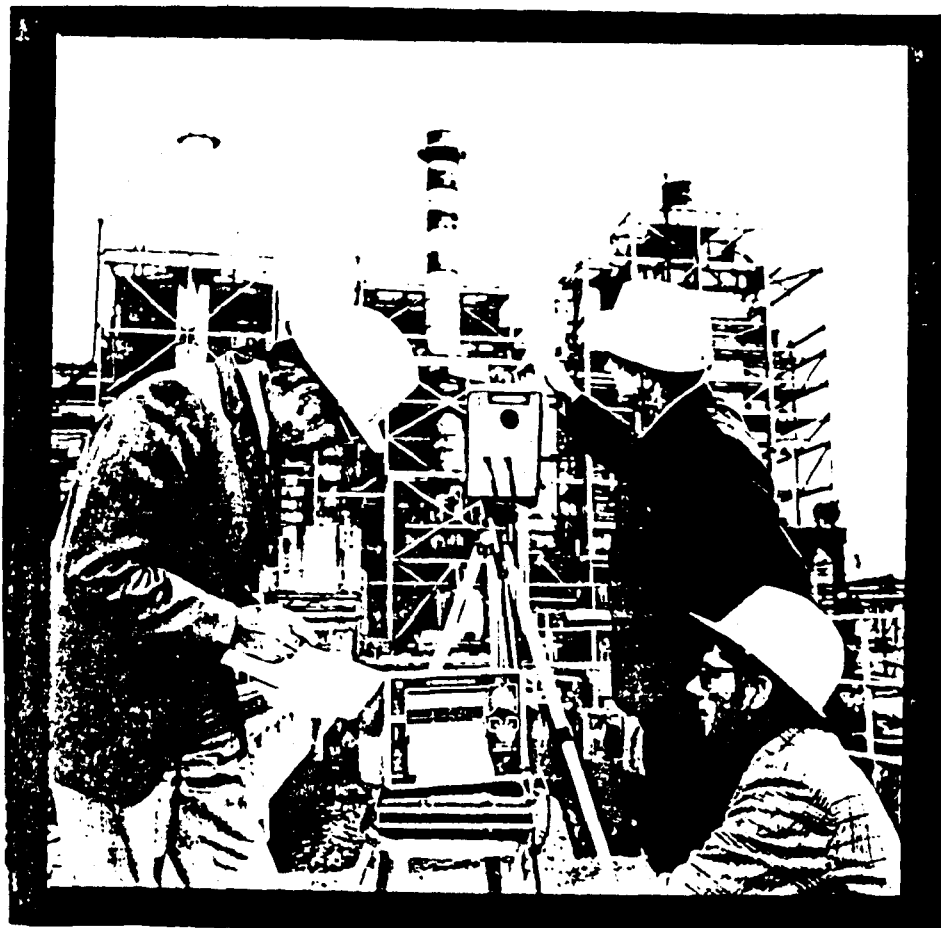


FIG. 14. Photograph of SO₂ remote sensor during initial field testing.

and analyzed following EPA Method 6; these data indicated SO₂ concentrations ranging from 30 to 50 ppm. However, the data were not believed reliable because of a leak in the sampling apparatus. Furthermore, the power plant company assumed 200 to 300 ppm were being emitted⁽⁷⁾, which is consistent with the observed results.

Field measurements were also made using the 1.0 x 1.0 mm detector and nearly-optimized gas cell parameters at a coal-burning power plant near Charlotte, N. C. A summary of the measurements is presented in Table 3.

TABLE 3
SUMMARY OF REMOTE SO₂ FIELD MEASUREMENTS
MADE AT A COAL-BURNING POWER PLANT

Date	Range	Stack Dia.	Fuel	Temp.	SO ₂ Conc. Range	Weather Conditions, Time
6/25/74	210 m	2.0 m	coal	425 K	700-1300 ppm	32 C, light wind, scattered clouds, p.
6/26/74	170 m	2.0 m	coal	425 K	700-1300 ppm	30 C, light wind, cloudy, a.m. and p.
6/27/74	170 m	2.0 m	coal	425 K	500-700 ppm	24 C, calm, foggy, a.m.
6/27/74	400 m	2.0 m	coal	425 K	500-700 ppm	24 C, calm, foggy, a.m.
6/27/74	210 m	2.0 m	coal	425 K	500-700 ppm	24 C, calm, rain, p.m.

Both radiometric and GFC mode of operation data were taken. In addition, extractive data were taken and analyzed following EPA Method 6 and continuously monitored by a DuPont Model 460-1 Analyzer⁽⁸⁾. All of the data are presented graphically in Figure 15. As seen, all of the data are in agreement within ± 100 ppm.

DISCUSSION OF FIELD TEST DATA REDUCTION

The data presented in Figure 15 were reduced by measuring the individual ΔV_1 and ΔV_2 signals because the signal levels were too low for the electronic divider module to function properly. In addition, the sensor was not perfectly balanced during the measurements. This means the terms (c. f. Equation (11))

$$\overline{N_p^0} \bar{\tau}_a (\tau_r - \bar{\tau}_o) \quad \text{and} \quad \overline{N_b^0} (1 - \bar{\tau}_a) (\tau_r - \bar{\tau}_o)$$

are not zero. Of these two terms the first term is much larger than the second term, and, the data were corrected by subtracting the contribution

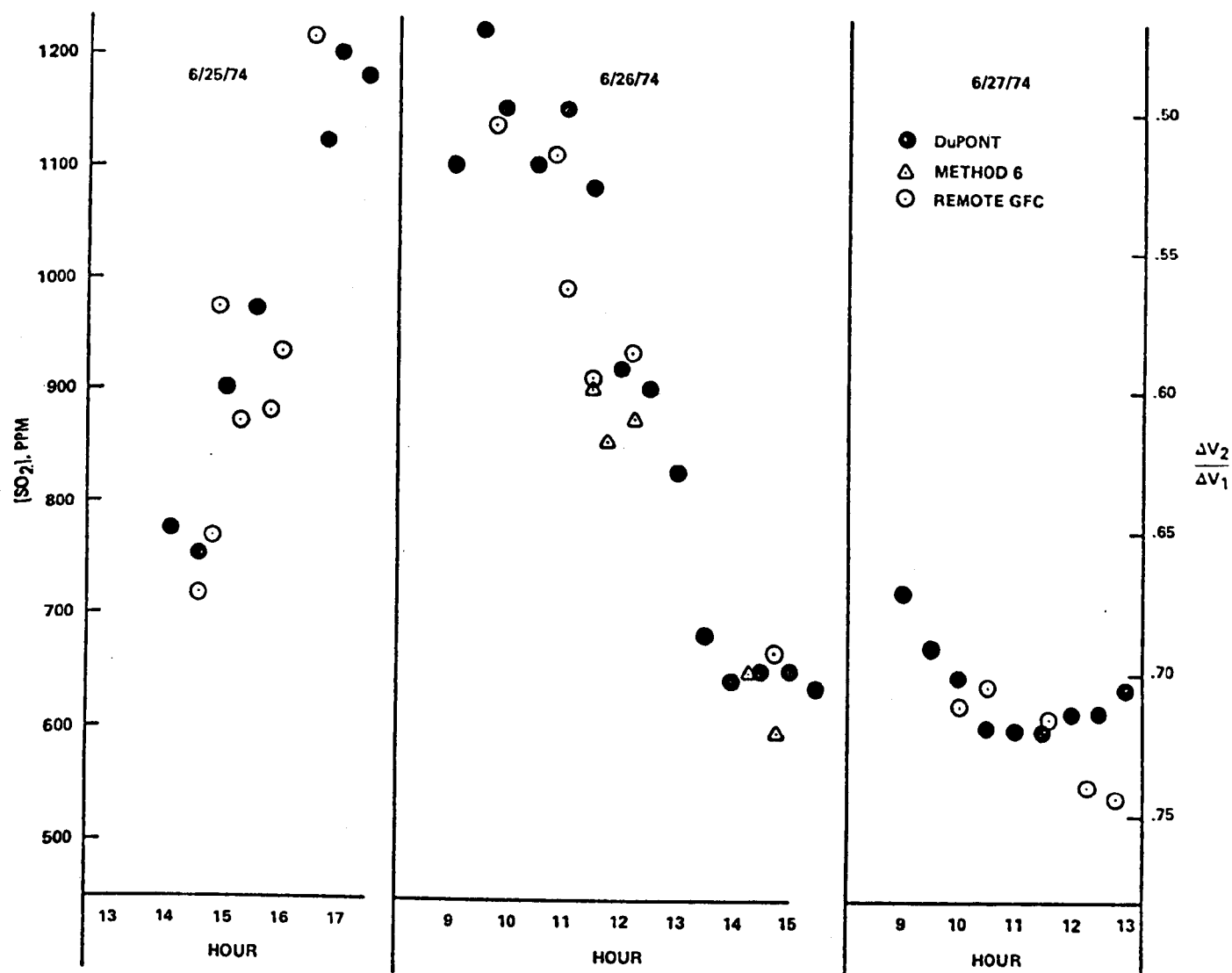


FIG. 15. Comparison of remote sensing data with extractive data obtained from the DuPont Analyzer and from EPA Method 6.

due to the first term. This contribution was measured in the laboratory using a blackbody field source both before and after the field measurements.

The majority of the measurements were averaged over about a 15 minute time period. In cases where the two ΔV signals were changing rapidly with time, the analyzed data was erratic and, thus, not used.

In the GFC mode, two principle sources of error arise. The first is due to the basic sensor sensitivity (signal-to-noise ratio) and the second due to the temperature dependent correction applied because of sensor imbalance, as noted above.

In the first case, the SNR averaged about 13 and 25 for channels ΔV_2 and ΔV_1 , respectively. Thus, for $u = 1600$ ppm-m, $\Delta V_2/\Delta V_1 = 0.55$, and in terms of error, this is equivalent to

$$\frac{\Delta V_2}{\Delta V_1} = \frac{0.55(1 \pm 1/13)}{1.0(1 \pm 1/25)} \quad (21)$$

which gives

$$\frac{\Delta V_2}{\Delta V_1} = 0.55 \pm 0.095 \quad (22)$$

Or, $u = 1600 \pm 350$ ppm-m and, at Location 2, this gives an uncertainty of ± 220 ppm in SO_2 concentration.

In the second case, it is believed that the plume temperature was known within ± 25 C. Note, in the cases where radiometric data were taken, it is believed to be known within ± 10 C. For temperature uncertainties of ± 10 and ± 25 C, the equivalent uncertainties in SO_2 concentration are about ± 70 and ± 175 ppm, respectively (on the average).

In summary, since both of these sources of uncertainties may be considered to be random, the maximum RSS uncertainty is about ± 280 ppm.

CONCLUSIONS

The GFC dual channel technique has been proven that it can remotely determine SO_2 concentrations in hot plumes with only minimal effects due to plume temperature and backgrounds. However, the prototype sensor was found to have certain limitations. These are:

1. Limited sensitivity due to detector noise.
2. A susceptibility to becoming unbalanced, which necessitates rather large temperature corrections.
3. Lack of provision for in-field rebalance adjustment capability.
4. Subject to erratic behavior due to overheating when operating in direct sunlight on very warm days.
5. The electronics divider module used does not permit electronic ratioing of the ΔV signals because of low signal levels.
6. A fov (8 mrads) that is larger than desired; 2 mrads would be better.

The deficiencies above were corrected by a modified design; this was done under EPA Contract 68-02-1696.

SECTION 4

REFERENCES

1. NASA Contracts 12-2109, 1-10466, 1-11111, and 1-12048.
2. Ludwig, C. B. et al., "Remote Measurement of Air Pollution by Nondispersive Optical Correlation", AIAA Paper No. 71-1107, November 1971; AIAA Jr. 11, 899, 1973.
3. Bartle, E. R. et al., "An In-Situ Monitor for HCl and HF", AIAA Paper No. 71-1049, November 1971; J. Spacecraft and Rockets, 11, 836, 1972.
4. Chandrasekhar, S., Radiative Transfer, Dover Publications, Inc. New York (1950).
5. Considine, D. M., Editor., Process Instruments and Controls Handbook, McGraw-Hill, New York (1957).
6. "Determination of Sulfur Dioxide Emissions from Stationary Sources", Federal Register 36, 24890, December 1971.
7. Hardway, J., SDG&E (private communication), March 1974.
8. The data obtained by the DuPont Model 460-1 Analyzer were provided by Dr. W. Herget of EPA.

APPENDIX

OPTIMIZATION OF GAS CELL PARAMETERS

THEORETICAL

A comparison of the two GFC calibration curves (Figures 11 and 12) shows a large increase in sensitivity to changes in SO₂ optical thickness when SO₂ is added to the reference cell. The signal-to-noise is actually decreased, but the sensitivity obtained when chopping between two cell pairs containing different optical thicknesses of SO₂ and ratioing is much greater than when chopping between two cell pairs, one of each containing different optical thicknesses of SO₂ and reference cells containing N₂.

For the latter case, the ratio is given by Equation (15); viz.

$$\frac{\Delta V_2}{\Delta V_1} = \frac{\overline{\tau\tau}_{02} - \overline{\tau\tau}_r f_2}{\overline{\tau\tau}_{01} - \overline{\tau\tau}_r f_1} \quad (\text{A-1})$$

Equation (A-1) reduces to Equation (14) when

$$\overline{\tau_r f_2} = \overline{\tau}_{02} \quad \text{and} \quad \overline{\tau_r f_1} = \overline{\tau}_{01}.$$

The mean value for transmissivity is given by

$$\overline{\tau} = \frac{1}{\Delta\lambda} \int_{\Delta\lambda} e^{-k(\lambda)u} d\lambda = \frac{1}{\Delta\lambda} \int_{\Delta\lambda} \sum_{n=0}^{\infty} \frac{(-1)^n}{n!} [k(\lambda)]^n u^n d\lambda \quad (\text{A-2})$$

where $u(\text{cm-atm})$ is the optical thickness and $k(\lambda)(\text{cm}^{-1}\text{-atm}^{-1})$ is the spectrally dependent absorption coefficient.

Since u is independent of wavelength,

$$\overline{\tau} = \sum_{n=0}^{\infty} \frac{(-1)^n}{n!} u^n \overline{k^n} \quad (\text{A-3})$$

Using Equations (A-1) and (A-3) for the case where $\tau_r = 1$ ($u_r = 0$)

$$\Delta V = \left[1 - \bar{k}(u + u_o) + \frac{\bar{k}^2}{2} (u + u_o)^2 - \frac{\bar{k}^3}{6} (u + u_o)^3 + \dots \right] \quad (A-4)$$

$$- \left[1 - \bar{k}u + \frac{\bar{k}^2}{2} u^2 - \frac{\bar{k}^3}{6} u^3 + \dots \right] \left[1 - \bar{k}u_o + \frac{\bar{k}^2}{2} u_o^2 - \frac{\bar{k}^3}{6} u_o^3 + \dots \right]$$

Simplifying, and considering only second order terms in u , gives

$$\Delta V = u \left\{ u_o (\bar{k}^2 - \bar{k}^2) - u_o^2 \left(\frac{1}{2} \right) (\bar{k} \bar{k}^2 - \bar{k}^3) + \dots \right\} \quad (A-5)$$

$$+ u^2 \left\{ u_o \left(\frac{1}{2} \right) (\bar{k} \bar{k}^2 - \bar{k}^3) - \dots \right\}$$

Defining

$$\bar{k}^2 - \bar{k}^2 \equiv A \quad \text{and} \quad \frac{1}{2} (\bar{k} \bar{k}^2 - \bar{k}^3) \equiv B \quad (A-6)$$

gives

$$\Delta V = u u_o [A - B(u + u_o)] \quad (A-7)$$

Considering the second cell pair, and forming the ratio between the two signals results in

$$\frac{\Delta V_2}{\Delta V_1} = \frac{u_{o2}}{u_{o1}} \left[\frac{A/B - (u + u_{o2})}{A/B - (u + u_{o1})} \right] \equiv f(u) \quad (A-8)$$

Differentiating Equation (A-8) with respect to u gives

$$f'(u) = \frac{u_{o2}}{u_{o1}} \cdot \frac{(u_{o1} - u_{o2})}{[A/B - (u + u_{o1})]^2} \quad (A-9)$$

which indicates the sensitivity with respect to u .

Considering now the case where there is gas in the reference cell of optical thickness, u_r , and transmissivity, τ_r , similar expressions can be derived. For this case, the modulation function, $\Delta V'$, is given by

$$\Delta V' = \overline{\tau} \overline{\tau}_0 - \overline{\tau} \overline{\tau}_r (\overline{\tau}_0 / \overline{\tau}_r) \quad (A-10)$$

Performing a similar series expansion to the second order in u gives

$$\begin{aligned} \Delta V' \left[e^{\overline{-k} u_r} \right] &= u \left\{ (u_0 - u_r) (\overline{k}^2 - \overline{k}) - (u_0^2 - u_r^2) \left(\frac{1}{2} \right) (\overline{k} \overline{k}^2 - \overline{k}^3) + \dots \right\} \\ &+ u^2 \left\{ (u_0 - u_r) (1/2) (\overline{k} \overline{k}^2 - \overline{k}^3) - \dots \right\} \end{aligned} \quad (A-11)$$

Again, considering the second cell pair, and forming the ratio between the two signals results in

$$\frac{\Delta V'_2}{\Delta V'_1} = \frac{(u_{02} - u_r)}{(u_{01} - u_r)} \cdot \left[\frac{A/B - (u_{02} + u_r + u)}{A/B - (u_{01} + u_r + u)} \right] \equiv F(u) \quad (A-12)$$

Differentiating Equation (A-12) with respect to u gives

$$F'(u) = \frac{(u_{02} - u_r)}{(u_{01} - u_r)} \cdot \frac{(u_{01} - u_{02})}{[A/B - (u_{01} + u_r + u)]^2} \quad (A-13)$$

Dividing Equation (A-13) by Equation (A-9) shows the relative effect in terms of sensitivity for the two cases; i. e.,

$$\frac{F'(u)}{f'(u)} = \frac{(u_{02} - u_r)}{(u_{01} - u_r)} \cdot \frac{(u_{01})}{(u_{02})} \cdot \frac{[A/B - (u_{01} + u)]^2}{[A/B - (u_{01} + u + u_r)]^2} \quad (A-14)$$

Equation (A-14) can be examined to show the increase in sensitivity to u in terms of the various cell optical thicknesses. Also, the fundamental equations, (A-7) (A-8), (A-11) and (A-12) can be examined to show the effect on signal levels.

The constant A/B was evaluated using the data presented in Figure 12. The results are as follows.

A/B (cm-atm)	Evaluated at
8.6	$F(0) = 0.95$
14.6	$F(u = 2000 \text{ ppm-m}) = 0.47$
9.1	$F'(0) = -2.5 \text{ cm}^{-1}\text{-atm}^{-1}$

This evaluation indicates A/B is not a constant and that the simplified analysis inadequately describes the true performance of the sensor. Nevertheless, calculations were made, assuming A/B = 12 cm-atm. The results are presented in Figure A-1. These curves indicate the dramatic improvement in sensitivity as the reference cell's optical thickness is increased. This can be seen by examination of Equation (A-14) since when

$$u_{01} + u + u_r = A/B \quad (\text{A-15})$$

the ratio of the sensitivity with $u_r \neq 0$ and sensitivity with $u_r = 0$ ($= F'(u)/f'(u)$) becomes infinite.

However, as was pointed out, this simplified analysis does not adequately describe the sensor's performance. This is principally due to not considering the higher order terms in the series expansion.

A similar analysis has been performed to include third order terms. The resulting equation is

$$F(u) \equiv \frac{u_{02} - u_r}{u_{01} - u_r} \times \frac{1 + (u_{02} + u_r + u)W + u_{02}u_rX + (u_{02}^2 + u_{02}u_r + u_r^2 + u^2)Y + (u_{02} + u_r)uZ}{1 + (u_{01} + u_r + u)W + u_{01}u_rX + (u_{01}^2 + u_{01}u_r + u_r^2 + u^2)Y + (u_{01} + u_r)uZ} \quad (\text{A-16})$$

The constants W, X, Y and Z have been evaluated by solving a 4 x 4 matrix using determinants developed from fitting the results presented in Figure 12. Their definitions and numerical values are given below.

$$\begin{aligned} W &= \frac{1}{2}(\bar{k} \bar{k}^2 - k^3)/(\bar{k}^2 - \bar{k}) = -0.3118 \\ X &= \frac{1}{2}(k^3 \bar{k} - \bar{k}^2)/(\bar{k}^2 - \bar{k}) = -0.0260 \\ Y &= \frac{1}{6}(k^4 - k^3 \bar{k})/(\bar{k}^2 - \bar{k}) = 0.0343 \\ Z &= \frac{1}{4}(k^4 - k^2)/(\bar{k}^2 - \bar{k}) = 0.0435 \end{aligned} \quad (\text{A-17})$$

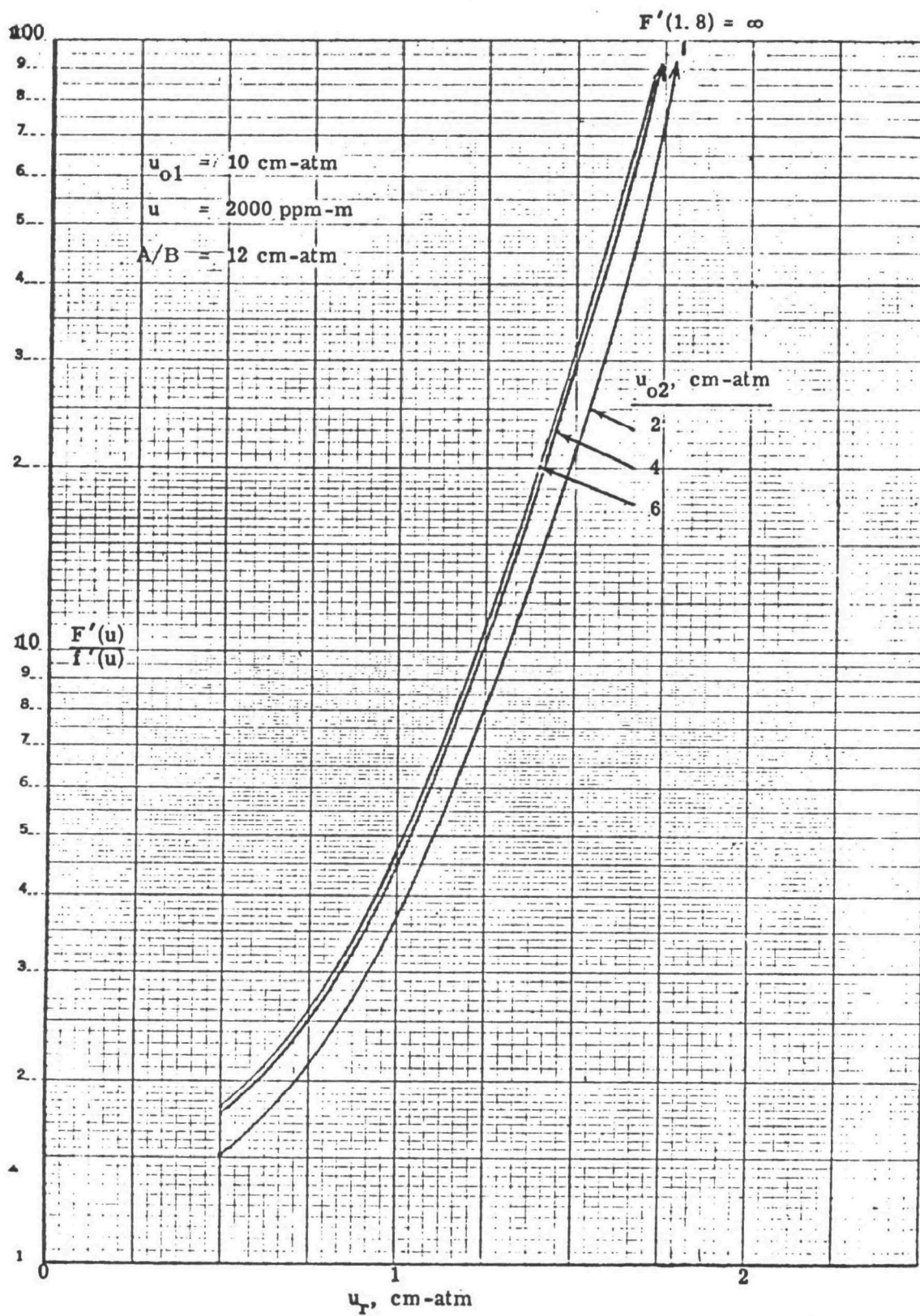


FIG. A-1. Effect of specifying and reference cell optical thickness on sensor sensitivity.

Using these values, the calibration data presented in Figure 12 is described within ± 2 percent over the range of 100 to 5000 ppm-m of SO_2 .

Calculations of ΔV for $u_o = 1, 2, 3, \dots, 10$ atm-cm and $u_r = 0, 0.5, 1.0, 1.5,$ and 2.0 atm-cm have been made. These results show how the addition of SO_2 to the reference cell affects the slope, but also reduces the signal intensity. It is calculated that at large specifying cell optical thicknesses, the signal levels are only reduced by about a factor of 2, even for large (2 atm-cm) amounts of SO_2 in the reference cell. It should also be noted that the results for intermediate specifying cell optical thicknesses (4 and 6 atm-cm) and reference cell optical thicknesses greater than 1 atm-cm, do not appear to be physically reasonable. This indicates that the use of the analytical expression is not quantitative enough. Apparently even higher order terms in the series approximation should be included. Nevertheless approximate optimum cell conditions have been calculated.

The expression for $F(u) = \Delta V_2 / \Delta V_1$ has been differentiated and numerically evaluated for $u = 1000$ ppm-m. These results show the rapid increase in sensitivity as the reference cell's optical thickness is increased and the optimum value for the second specifying cell's optical thickness. Furthermore, they indicate that the sensitivity, $F'(u)$, continues to increase as u_{o1} increases.

Since the length of both specifying cells in the sensor is 10 cm and it is undesirable to pressurize the SO_2 beyond one atmosphere due to pressure broadening the SO_2 lines, the practical maximum optical thickness for u_{o1} is 10 atm-cm. For this condition, the calculations indicate the optimum value for the second specifying cell's optical thickness is about 4.5 atm-cm.

We have also calculated the values for the reference cell's optical thickness that forces $F'(u) \rightarrow \infty$ for $u = 1000$ ppm-m; the result is $u_r = 1.8$ atm-cm.

In summary, calculations made using the third order series expansion analysis indicate the sensor would have optimum performance with

$$u_{o1} = 10 \text{ atm-cm}$$

$$u_{o2} = 4.5 \text{ atm-cm}$$

$$u_r = 1.8 \text{ atm-cm}.$$

EXPERIMENTAL

Measurements have been made using the sensor to determine SO_2 transmissivity as a function of optical thickness. The sensor was operated in the radiometric mode by blocking off the reference cell apertures. The

lower specifying cell was evacuated, and the signal (I_0) recorded; then, pre-mixed SO_2 diluted with N_2 was admitted to the cell at one atmosphere pressure and the signal (I) recorded. The ratio I/I_0 is, of course, the transmissivity. The results of this experiment was presented in Figure A-2. Also shown are the results generated by a line-by-line computer program using the actual filter function of the sensor.

Laboratory calibrations of the sensor operating in the GFC mode are difficult. We used a 50 cm long cell with sapphire windows on both ends providing a clear aperture of 6.2 cm. The windows are uncoated and have a transmissivity of 0.88. The maximum entrance aperture dimension is $(0.775 + 0.867)(2.54) = 4.17$ cm. Locating the sensor 100 cm away from the far end window of the cell gives a projected maximum dimension of $4.17 + (.008)(100) = 4.97$ cm and, thus, no direct contribution is given by the cell walls. However, three major difficulties arise in the calibration.

One. Multiple reflections internal to the cell and near field-of-view thermal non-uniformities generally give unreliable ΔV signals.

Two. The cell is heated by external strip heaters, cold pre-mixed SO_2 - N_2 test gas mixtures are admitted to the cell and the temperature monitored by a thermocouple in the cell's interior. It is difficult to maintain the same temperature as different SO_2 - N_2 concentrations are sequentially admitted to the cell and maintained at one atm pressure. Since the temperature strongly affects the magnitude of the ΔV signals and relatively long time constants (30 seconds) are required to get adequate signal-to-noise, the data tend to be erratic.

Three. Field data give ΔV signals that are larger than those simulated in the laboratory and indicate a greater sensitivity to changes in SO_2 optical thickness.

The most desirable methods for calibrating the sensor appears to be the use of field data or to use an artificial stack. For SO_2 optical thicknesses greater than 5000 ppm-m, laboratory measurements generally give repeatable results if the temperatures and concentrations of test gas mixtures are carefully controlled.

In attempting to simulate the theoretically predicted optimum gas cell parameters, it was discovered that for $u_{01} = 10$ and $u_r = 1.8$ cm-atm of SO_2 , respectively, the throughput (and signal) of the sensor was reduced by 70 percent (see Figure A-2) and the aperture adjustment did not have enough travel to balance the sensor.

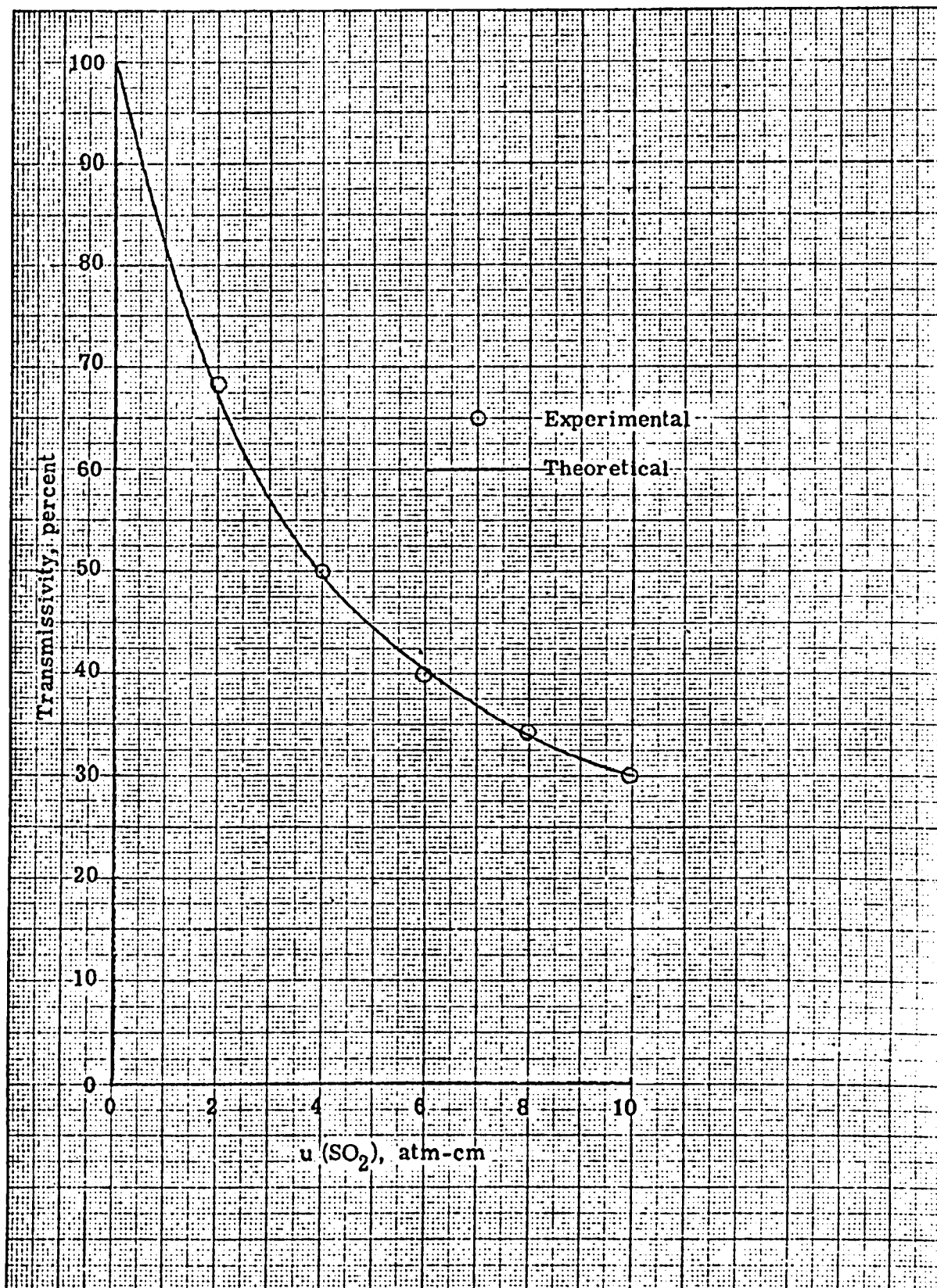


FIG. A-2. Theoretical calculation and measurement of N_2 -diluted SO_2 pressurized to one atm for SO_2 sensor.

Within the limits of the sensor's balancing adjustment and the repeatable signals generated using the calibration cell, the apparent optimum cell parameters were determined and are summarized below.

Parameter	Upper Cell, ΔV_2	Lower Cell, ΔV_1	Reference Cell
Chopping frequency	40 Hz	100 Hz	40 and 100 Hz
Length	10 cm	10 cm	23 cm
SO ₂ Concentration	17.2 %	47.2 %	2.2 %
Optical thickness	2.0 atm-cm	5.0 atm-cm	0.5 atm-cm
Transmissivity	0.66	0.44	0.88

Note, the sensor's construction is such that the two 10 cm long specifying cells and the 23 cm long reference cell actually give effective u_o 's that are the sum of the SO₂ pressure in the specifying cell times 10 cm plus the SO₂ pressure in the reference cell times 13.

TECHNICAL REPORT DATA
(Please read Instructions on the reverse before completing)

1. REPORT NO. EPA-650-2-75-041		2.		3. RECIPIENT'S ACCESSION NO.	
4. TITLE AND SUBTITLE Infrared Sensor for Remote Monitoring of SO₂				5. REPORT DATE May 1975	
				6. PERFORMING ORGANIZATION CODE	
7. AUTHOR(S) E. R. Bartle and E. A. Meckstroth				8. PERFORMING ORGANIZATION REPORT NO.	
9. PERFORMING ORGANIZATION NAME AND ADDRESS JRB Associates, Division of SAI 1200 Prospect Street P. O. Box 2351 La Jolla, CA 92037				10. PROGRAM ELEMENT NO. 1AA010	
				11. CONTRACT/GRANT NO. 68-02-1208	
12. SPONSORING AGENCY NAME AND ADDRESS National Environmental Research Center Office of Research and Development U. S. Environmental Protection Agency Research Triangle Park, N. C. 27711				13. TYPE OF REPORT AND PERIOD COVERED Final Report	
				14. SPONSORING AGENCY CODE	
15. SUPPLEMENTARY NOTES					
16. ABSTRACT <p>A prototype passive infrared sensor for the measurement of sulfur dioxide emissions from stationary sources is described. The infrared radiation emitted by gases in a plume originating from smokestacks may be detected, and from this the SO₂ concentration in the plume may be determined. In general, the radiation received by the sensor is a function of the intervening and background atmosphere. Thus, the problem of quantitative measurements is generally complex. A technique is described, based upon the principle of Gas Filter Correlation, which minimizes these effects.</p> <p>This report presents a detailed description of the sensor, it's specifications, and performance characteristics. The basic unit is battery operated and weighs only 10 kgms; thus, it is readily portable. It's sensitivity is presently limited to about 70 ppm-m for source plume temperatures of 270 C and about 290 ppm-m for temperatures of 170 C, but this can be improved.</p> <p>The results of field testing at both oil and coal-burning power plants are compared with extractive sample data. In general, the remote measurements agree with the extractive data within ± 25 percent over SO₂ concentrations ranging from 150 ppm to 1300 ppm from slant ranges of 130 to 400 m.</p> <p>This report is submitted in partial fulfillment of contract number 68-02-1208 by JRB Associates, a division of Science Applications, Inc. under the sponsorship of the Environmental Protection Agency.</p>					
17. KEY WORDS AND DOCUMENT ANALYSIS					
a. DESCRIPTORS		b. IDENTIFIERS/OPEN ENDED TERMS		c. COSATI Field/Group	
1. Remote Sensing 2. SO ₂ Measurements 3. Gas Filter Correlation					
18. DISTRIBUTION STATEMENT Release Unlimited		19. SECURITY CLASS (This Report) Unclassified		21. NO. OF PAGES 45	
		20. SECURITY CLASS (This page) Unclassified		22. PRICE	

INSTRUCTIONS

1. **REPORT NUMBER**
Insert the EPA report number as it appears on the cover of the publication.
2. **LEAVE BLANK**
3. **RECIPIENTS ACCESSION NUMBER**
Reserved for use by each report recipient.
4. **TITLE AND SUBTITLE**
Title should indicate clearly and briefly the subject coverage of the report, and be displayed prominently. Set subtitle, if used, in smaller type or otherwise subordinate it to main title. When a report is prepared in more than one volume, repeat the primary title, add volume number and include subtitle for the specific title.
5. **REPORT DATE**
Each report shall carry a date indicating at least month and year. Indicate the basis on which it was selected (*e.g., date of issue, date of approval, date of preparation, etc.*).
6. **PERFORMING ORGANIZATION CODE**
Leave blank.
7. **AUTHOR(S)**
Give name(s) in conventional order (*John R. Doe, J. Robert Doe, etc.*). List author's affiliation if it differs from the performing organization.
8. **PERFORMING ORGANIZATION REPORT NUMBER**
Insert if performing organization wishes to assign this number.
9. **PERFORMING ORGANIZATION NAME AND ADDRESS**
Give name, street, city, state, and ZIP code. List no more than two levels of an organizational hierarchy.
10. **PROGRAM ELEMENT NUMBER**
Use the program element number under which the report was prepared. Subordinate numbers may be included in parentheses.
11. **CONTRACT/GRANT NUMBER**
Insert contract or grant number under which report was prepared.
12. **SPONSORING AGENCY NAME AND ADDRESS**
Include ZIP code.
13. **TYPE OF REPORT AND PERIOD COVERED**
Indicate interim final, etc., and if applicable, dates covered.
14. **SPONSORING AGENCY CODE**
Leave blank.
15. **SUPPLEMENTARY NOTES**
Enter information not included elsewhere but useful, such as: Prepared in cooperation with, Translation of, Presented at conference of, To be published in, Supersedes, Supplements, etc.
16. **ABSTRACT**
Include a brief (*200 words or less*) factual summary of the most significant information contained in the report. If the report contains a significant bibliography or literature survey, mention it here.
17. **KEY WORDS AND DOCUMENT ANALYSIS**
 - (a) **DESCRIPTORS** - Select from the Thesaurus of Engineering and Scientific Terms the proper authorized terms that identify the major concept of the research and are sufficiently specific and precise to be used as index entries for cataloging.
 - (b) **IDENTIFIERS AND OPEN-ENDED TERMS** - Use identifiers for project names, code names, equipment designators, etc. Use open-ended terms written in descriptor form for those subjects for which no descriptor exists.
 - (c) **COSATI FIELD GROUP** - Field and group assignments are to be taken from the 1965 COSATI Subject Category List. Since the majority of documents are multidisciplinary in nature, the Primary Field/Group assignment(s) will be specific discipline, area of human endeavor, or type of physical object. The application(s) will be cross-referenced with secondary Field/Group assignments that will follow the primary posting(s).
18. **DISTRIBUTION STATEMENT**
Denote releasability to the public or limitation for reasons other than security for example "Release Unlimited." Cite any availability to the public, with address and price.
19. & 20. **SECURITY CLASSIFICATION**
DO NOT submit classified reports to the National Technical Information service.
21. **NUMBER OF PAGES**
Insert the total number of pages, including this one and unnumbered pages, but exclude distribution list, if any.
22. **PRICE**
Insert the price set by the National Technical Information Service or the Government Printing Office, if known.